EUROPEAN ORGANIZATION FOR NUCLEAR RESEARCH (CERN)

CERN-EP-2022-005
2022/05/05

CMS-GEN-17-002

CMS PYTHIA 8 colour reconnection tunes based on underlying-event data

The CMS Collaboration

Abstract

New sets of parameter tunes for two of the colour reconnection models, quantum chromodynamics-inspired and gluon-move, implemented in the PYTHIA 8 event generator, are obtained based on the default CMS PYTHIA 8 underlying-event tune, CP5. Measurements sensitive to the underlying event performed by the CMS experiment at centre-of-mass energies $\sqrt{s} = 7$ and 13 TeV, and by the CDF experiment at 1.96 TeV are used to constrain the parameters of colour reconnection models and multiple-parton interactions simultaneously. The new colour reconnection tunes are compared with various measurements at 1.96, 7, 8, and 13 TeV including measurements of the underlying-event, strange-particle multiplicities, jet substructure observables, hadron ratios (from e^+e^- colliders), jet shapes, and colour flow in top quark pair ($t\bar{t}$) events. The new tunes are also used to estimate the uncertainty related to colour reconnection modelling in the top quark mass measurement using the decay products of $t\bar{t}$ events in the semileptonic channel at 13 TeV.

Submitted to the European Physical Journal C

1 Introduction

Monte Carlo (MC) event generators, such as PYTHIA 8 [1], are indispensable tools for measurements at the LHC proton-proton (pp) collider. To provide an accurate description of high-energy collisions, both the hard scattering and the so-called underlying event (UE) are computed for each simulated event. In the hard scattering process, two initial partons interact with a large exchange of transverse momentum ($p_{\mathrm{T}} > \mathcal{O}(\mathrm{GeV})$). The UE represents additional activity occurring at lower energy scales that accompany the hard scattering. It consists of multiple-parton interactions (MPIs), initial- and final-state radiation (ISR and FSR), and beam-beam remnants (BBR). According to Quantum Chromodynamics (QCD), strong interactions are affected by colour charges that are carried by quarks and gluons. All of the coloured partons produced by these components are finally combined to form colourless hadrons through the hadronisation process.

Particularly relevant for the characterisation of the UE are the MPI, which consist of additional 2-to-2 parton-parton interactions occurring within the single collision event. With increasing collision energy, the interaction probability for partons at small longitudinal momentum fractions also increases, which enhances MPI contributions.

The PYTHIA 8 generator regularises the cross sections of the primary hard scattering processes and MPIs with respect to the perturbative 2-to-2 parton-parton differential cross section through an energy-dependent dampening parameter p_{T0}, which depends on the centre-of-mass energy $\sqrt{s}$. The energy dependence of the p_{T0} parameter in PYTHIA 8 is described with a power law function of the form

$$p_{\mathrm{T0}}(\sqrt{s}) = p_{\mathrm{T0}}^{\mathrm{ref}} \left(\frac{\sqrt{s}}{\sqrt{s_0}} \right)^{\epsilon}, \tag{1}$$

where $p_{\mathrm{T0}}^{\mathrm{ref}}$ is the value of p_{T0} at a reference energy $\sqrt{s_0}$, and ϵ is a tunable parameter that determines the energy dependence. At a given $\sqrt{s}$, the mean number of additional interactions from MPI depends on p_{T0}, the parton distribution functions (PDFs), and the overlap of the matter distributions of the two colliding hadrons [2].

To track the colour information during the development of the parton shower, partons are represented and also connected by colour lines. Quarks and antiquarks are represented by colour lines with arrows pointing in the direction of the colour flow, and gluons are represented by a pair of colour lines with opposite arrows. Rules for colour propagation are shown in Fig. 1. Because each MPI system adds coloured partons to the final state, a dense net of colour lines that overlap with the coloured parton fields of the hard scattering and with each other is created. Parton shower algorithms, in general, use the leading colour (LC) approximation [3, 4] in which each successively emitted parton is colour connected to its parent emitter in the limit of infinite number of colours. Colour reconnection (CR) models allow colour lines to be formed between partons also from different interactions and thus allow different colour topologies compared with a simple LC approach.

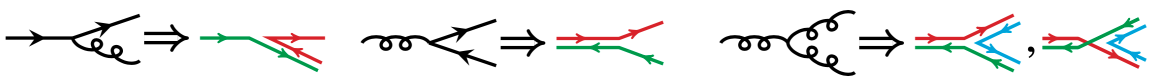

Figure 1: Rules for colour flow for quark-gluon vertices. Figure is taken from Ref. [5]. Quark-gluon vertices are shown in black with Feynman diagrams and colour connection lines are shown with coloured lines.

The CR was first included in minimum-bias (MB) simulations to reproduce the increase of average transverse momentum $\langle p_{\mathrm{T}} \rangle$ of charged particles as a function of the multiplicity of

the measured charged particles, N_{ch}, and also to describe the $dN_{ch}/d\eta$ distribution [6, 7]. The pseudorapidity is defined as $\eta = -\ln[\tan(\theta/2)]$, where the polar angle θ is defined with respect to the anticlockwise-beam direction. Introducing correlations between partons, including those also resulting from MPIs, generally changes the number of charged particles in an event and allows a more realistic simulation of charged-particle multiplicity and $\langle p_T \rangle$ vs N_{ch} distributions than in an event scenario without CR [7].

Various phenomenological models for CR have been developed and are included in simulations. In these models, the general idea is to determine the partonic configuration that reproduces the minimal total string length. Then, the obtained partonic configuration is passed on to the subsequent hadronisation process.

None of the MPI processes or the CR models are completely determined from first principles, and they all include free parameters. A specified set of such parameters that is adjusted to better fit some aspects of the data is referred to as a "tune". This paper presents results from two tunes, which make use of the QCD-inspired [8] and the gluon-move [9] CR models. The new CR tunes presented are based on the default CMS PYTHIA 8 tune CP5 [10]. Along with the CP5 tune, which is derived from the MPI-based CR model, the performance of the new CR tunes (CP5-CR1 and CP5-CR2 defined below) is studied using several observables. These tunes can be used for the evaluation of the uncertainties due to CR effects, and deepening the understanding of the CR mechanism.

The paper is organised as follows. In Section 2, the different colour reconnection models implemented in PYTHIA 8 and used in this study are introduced. In Section 3, the tuning strategy is explained in detail and the parameters of the new tunes are presented. Section 4 shows a selection of validation plots related to observables measured at $\sqrt{s} = 1.96$, 7, 8, and 13 TeV compared with the predictions of the new tunes. In Section 5 a study of the uncertainty in the top quark mass m_t measurement because of the CR modelling is presented before summarising the results in Section 6.

2 Colour reconnection models

The MPI-based CR model [6] was the only CR model implemented in PYTHIA 8 until PYTHIA 8.2, which was released with two additional CR models. The models implemented in PYTHIA 8.2, referred to as the "MPI-based", "QCD-inspired", and "gluon-move" CR models, are briefly described in the following:

- *MPI-based model (CP5):* the simplest model [11] implemented in MC event generators introduces only one tunable parameter. In this model, the partons are classified according to the MPI system to which they belong. Each parton interaction is originally a $2 \to 2$ scattering. For an MPI system with a hardness scale p_T of the $2 \to 2$ interaction, a CR probability is defined as:

$$P = \frac{p^2_{T_{Rec}}}{(p^2_{T_{Rec}} + p^2_T)}, \tag{2}$$

  with $p_{T_{Rec}} = r p_{T0}$, where r is a tunable parameter and p_{T0} is an energy-dependent dampening parameter used for the MPI description. The parameter p_{T0} avoids a divergence of the partonic cross section at low p_T. According to Eq.(2), MPI systems at high p_T would tend to escape from the interaction point, without being colour reconnected to the hard scattering system. Colour fields originating from a low-p_T

MPI system would instead more likely exchange colour. Once the systems to be connected are determined, partons of low-p_{T} systems are added to strings defined by the highest p_{T} system to achieve a minimal total string length.

- *QCD-inspired model (CP5-CR1):* the QCD-inspired model [8] implemented in PYTHIA 8 adds the QCD colour rules on top of the minimisation of the string length. The model constructs all pairs of QCD dipoles allowed to be reconnected by QCD colour rules that determine the colour compatibility of two strings. This is done iteratively until none of the allowed reconnection possibilities result in a shortening of the total string length. It uses a simple picture to causally connect the produced strings in spacetime through a string length measure λ to determine favoured reconnections. The default parametrisation for λ is

$$\lambda = \ln\left(1 + \sqrt{2}\frac{E_1}{m_0}\right) + \ln\left(1 + \sqrt{2}\frac{E_2}{m_0}\right), \tag{3}$$

  where E_1 and E_2 represent the energies of the coloured partons in the rest frame of the QCD dipole, and m_0 is a constant with the dimension of energy [8]. Additionally, the QCD-inspired model allows for the creation of junction structures, which give the possibility of including higher-order effects in CR. Junctions are not simply QCD dipoles; they can be directly produced by three or four QCD dipoles. This new CR model allows different colour topologies beyond the LC according to the rules described above.

- *Gluon-move model (CP5-CR2)*: in this scheme [9], final-state gluons are identified along with all the colour-connected pairs of partons. Then an iterative process starts. The difference between string lengths when a final-state gluon belonging to two connected partons is moved to another connected two-parton system is calculated. The gluon is moved to the string for which the move gives the largest reduction in total string length. This procedure can be repeated for all or a fraction of the gluons in the final state, which is controlled by the PYTHIA 8 parameter `ColourReconnection:fracGluon`.

  In this scheme, quarks would not be reconnected, i.e. they would remain in the same position without any colour exchange. To improve this picture, the flip mechanism of the gluon-move model can be included. The flip mechanism basically allows reconnection of two different string systems, i.e. a quark can connect to a different antiquark. Junctions (Y-shaped three-quark configurations) are allowed to take part in the flip step as well, but no considerable differences are expected due to the limitation of the junction formation in this model. The flip mechanism has not been extensively studied and its effect on diffractive events is not known. For this reason the flip mechanism is switched off in PYTHIA 8 and not used in this paper. The main free parameters of the gluon-move model account for the lower limit of the string length allowed for colour reconnection, the fraction of gluons allowed to move, and the lower limit of the allowed reduction of the string lengths.

In addition to these models, the effects of early resonance decay (ERD) [9] in top quark decays are also studied. With this option, top quark decay products are allowed to participate directly in CR. Normally the ERD option is switched off in PYTHIA 8 but in Section 4.5 we investigate the ERD effects.

Usually, MPI and CR effects are investigated and constrained using fits to measurements sensitive to the UE in hadron collisions. The UE measurements have been performed at various collision energies by ATLAS, CMS, and CDF Collaborations [12–16]. The measurements are

typically performed by studying the multiplicity and the scalar p_{T} sum of the charged particles ($p_{\mathrm{T}}^{\mathrm{sum}}$), measured as a function of the p_{T} of the leading charged particle in the event.

Different regions of the plane transverse to the direction of the beams are defined by the direction of the leading charged particle. A sketch of the different regions is shown in Fig. 2. A "toward" region includes mainly the products of the hard scattering, whereas the "away" region includes the recoiling objects belonging to the hard scattering. The two "transverse" regions contain the products of MPIs and are affected by contributions from ISR and FSR.

Recent measurements [12, 13, 16] subdivide the transverse region into "transMIN" and "transMAX", defined to be the regions with the minimum and maximum number of particles between the two transverse regions. This is done to disentangle contributions from MPI, ISR, and FSR. For events with large ISR or FSR, the transMAX region contains at least one "transverse-side" jet, whereas both the transMAX and transMIN regions contain particles from the MPI and BBR. Thus, the transMIN region is sensitive to the MPI and BBR, whereas the transMAX minus the transMIN is sensitive to ISR and FSR.

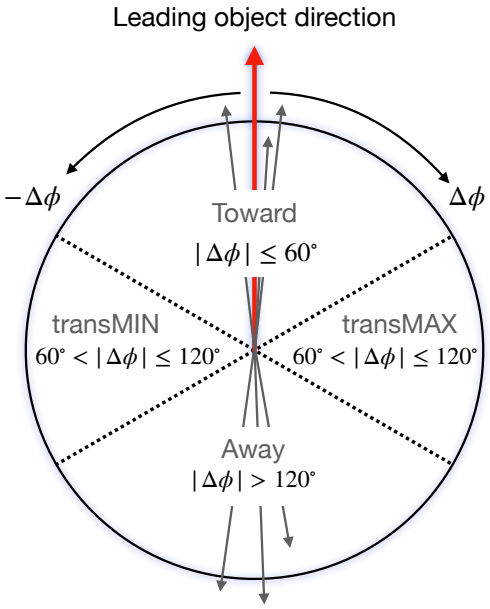

Figure 2: The schematic description of the result of a typical hadron-hadron collision. The "toward" region contains the "toward-side" jet, whereas the "away" region may contain an "away-side" jet.

The CMS Collaboration showed that a consistent description of the N_{ch} and the $p_{\mathrm{T}}^{\mathrm{sum}}$ distributions is not possible using only the PYTHIA 8 hadronisation model without taking into account the CR effects [17]. In general, the largest difference between the predictions from tunes and the data is observed in the soft region ($p_{\mathrm{T}} \sim$ 2–5 GeV), where CR effects are expected to be more relevant. The CR effects are also important for processes occurring at larger scales in pp collisions. In $\mathrm{t\bar{t}}$ events, the inclusion of CR effects can lead to a significant improvement in the description of UE variables [18]. The effects of CR may become more prominent in precision measurements, such as m_{t}. Uncertainties in m_{t} related to CR are usually estimated from comparing the prediction of a given model with and without CR, which might underestimate their effect [9]. A better way to approach the uncertainty estimation would be to consider a variety of CR models and variations of their parameters [19], which probe the effects of the underlying soft physics of pp collisions on the relevant observable.

The new CR models, QCD-inspired and gluon-move, were implemented in PYTHIA 8.226 after tuning the model parameters to the existing data at $\sqrt{s} = 7$ TeV and at lower centre-of-mass energies [8, 9]. The model predictions, with their default parameter settings in PYTHIA 8.226 and CP5, are given in Fig. 3 for charged particle and $p_{\mathrm{T}}^{\mathrm{sum}}$ densities measured by the CMS experiment at 13 TeV [12] in the transMIN and transMAX regions, and in Fig. 4 for the charged hadron pseudorapidity distribution, $\mathrm{d}N_{\mathrm{ch}}/\mathrm{d}\eta$, measured by CMS at 13 TeV [20]. In these figures, the data points are shown in black. These comparisons show that the models must be retuned to describe the underlying soft physics of pp collisions at 13 TeV.

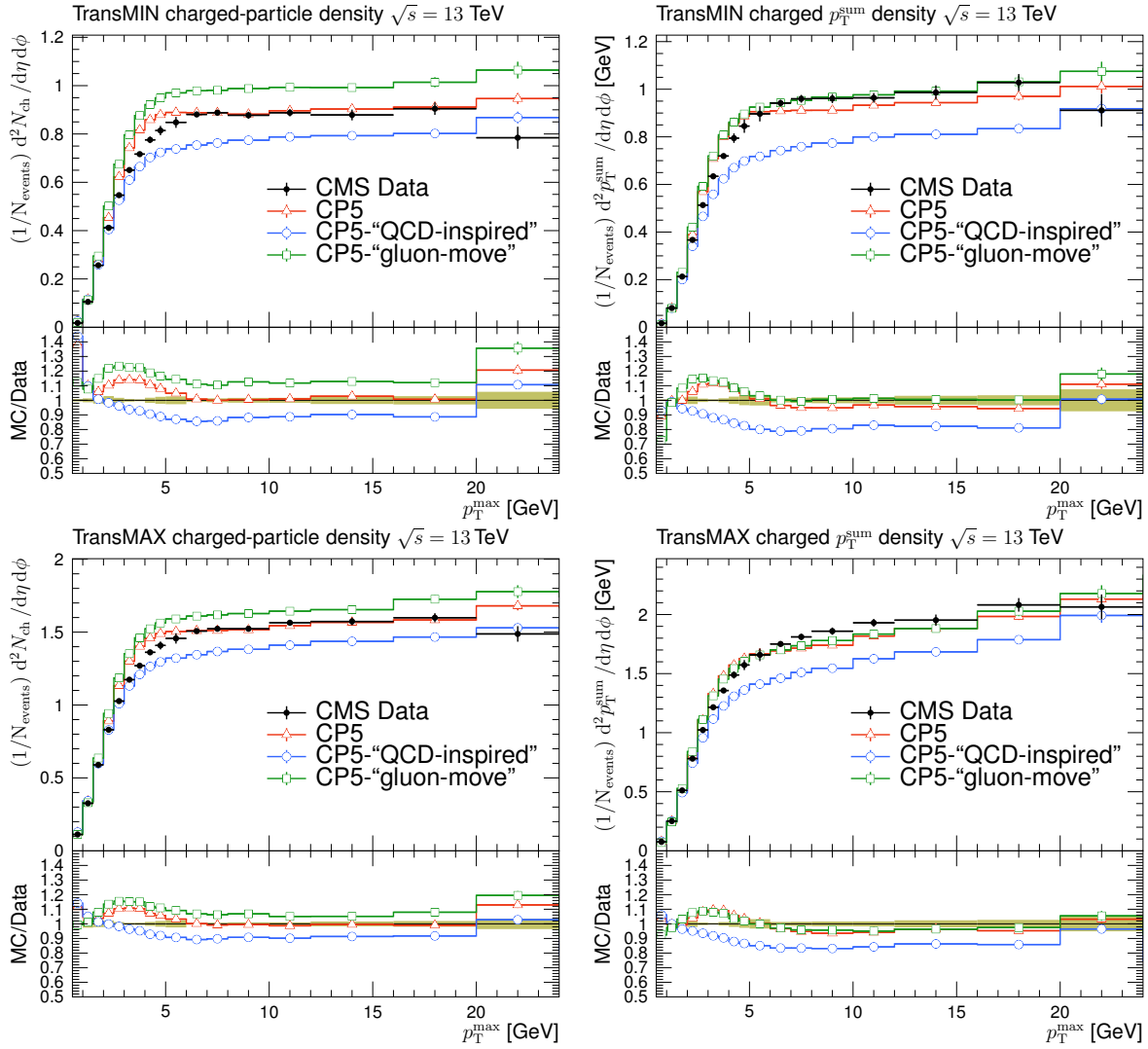

Figure 3: The charged-particle (left) and $p_{\mathrm{T}}^{\mathrm{sum}}$ densities (right) in the transMIN (upper) and transMAX (lower) regions as functions of the p_{T} of the leading charged particle, $p_{\mathrm{T}}^{\mathrm{max}}$, measured by the CMS experiment at $\sqrt{s} = 13$ TeV [12]. The predictions of the tunes CP5, CP5-"QCD-inspired", and CP5-"gluon-move" using their default parameter settings in Refs. [8, 9], are compared with data. The coloured band and error bars on the data points represent the total experimental uncertainty in the data where the model uncertainty is also included. The comparisons show that the models do not describe the data and need to be retuned.

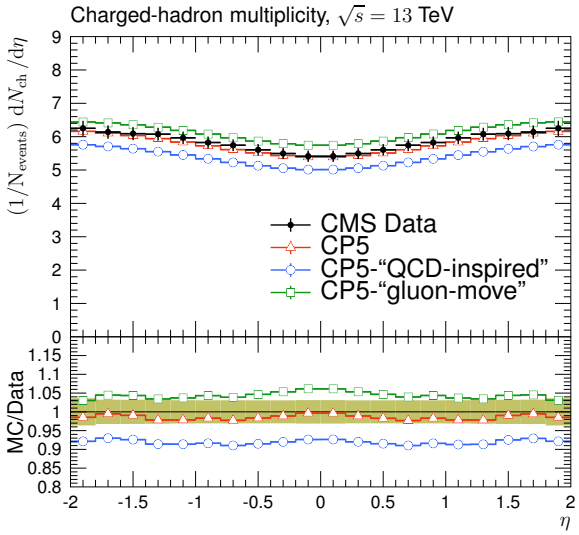

Figure 4: The pseudorapidity of charged hadrons, $dN_{ch}/d\eta$, measured in $|\eta| < 2$ by the CMS experiment at $\sqrt{s} = 13$ TeV [21]. The predictions of the tunes CP5, CP5-"QCD-inspired", and CP5-"gluon-move" using their default parameter settings in Refs. [8, 9], are compared with data. The coloured band and error bars on the data points represent the total experimental uncertainty in the data where model uncertainty is also included. The comparisons show that the models need to be retuned in order to have a better agreement with the data.

3 The new CMS colour reconnection tunes

A new set of event tunes, based on UE data from the CMS and CDF experiments, are derived using the QCD-inspired and the gluon-move CR models, as implemented in the PYTHIA 8.226 event generator. Having tunes for different CR models allows a consistent way of evaluating systematic uncertainties because of colour reconnection effects in specific measurements. The RIVET 2.4.0 [22] routines used as inputs to the fits, as well as the centre-of-mass energy values and the names of the RIVET distributions, the x-axis ranges (fit ranges), and the relative importance (R) of the distributions are displayed in Table 1 for the tunes CP5-CR1 and CP5-CR2. The CP5 tune is used as a baseline for the CR tuning since it is the default PYTHIA 8 tune for most of the new CMS analyses using data at $\sqrt{s} = 13$ TeV published since 2017, and it has explicitly been tested against a large number of different final states (MB, QCD, top quark, and vector boson + jets) and observables [10].

The parameters and their ranges in the fits are shown in Table 2. The minimum and maximum values of the parameters are first taken from PYTHIA 8, then the ranges of the values are further limited using the PROFESSOR 1.4.0 software [23]. The ranges are chosen such that the sampled MC space does not destroy the definition of a particular observable in the fits.

Tune CP5 uses the NNPDF31_nnlo_as_0118 [24] PDF set, the strong coupling parameter α_S value of 0.118 for ISR, FSR, and MPI, and the MPI-based CR model. It also uses a double-Gaussian functional form with two tunable parameters, `coreRadius` and `coreFraction`, to model the overlap of the matter distribution of the two colliding protons. The tune parameters are documented in Ref. [10] and displayed in Table 3.

The new tunes are obtained by constraining simultaneously the parameters controlling the contributions of the MPI and of each of the CR models. The strategy followed to obtain the CP5-CR1 and CP5-CR2 tunes is similar to that used for the CP5 tune, i.e. the same observables sensitive to MPI are considered to constrain the parameters. These are the N_{ch} and average

Table 1: List of input RIVET routines, centre-of-mass energy values, η ranges, names of distributions, fit ranges, and relative importance of the distributions used in the fits to derive the tunes CP5-CR1 and CP5-CR2.

				CP5-CR1		CP5-CR2	
RIVET routine	$\sqrt{s}$ [TeV]	$\lvert\eta\rvert$	Distribution	Fit range [GeV]	R	Fit range [GeV]	R
CMS_2015_I1384119	13	<2.0	N_{ch} versus η		1		1
CMS_2015_PAS_FSQ_15_007	13	<2.0	TransMIN charged p_T^{sum}	2–28	1	3–36	0.5
			TransMAX charged p_T^{sum}	2–28	1	3–36	0.5
			TransMIN N_{ch}	2–28	1	3–36	0.1
			TransMAX N_{ch}	2–28	1	3–36	0.1
CMS_2012_PAS_FSQ_12_020	7	<0.8	TransMAX N_{ch}	3–20	1	3–20	0.1
			TransMIN N_{ch}	3–20	1	3–20	0.1
			TransMAX charged p_T^{sum}	3–20	1	3–20	0.1
			TransMIN charged p_T^{sum}	3–20	1	3–20	0.1
CDF_2015_I1388868	2	<0.8	TransMIN N_{ch}	2–15	1	2–15	0.1
			TransMAX N_{ch}	2–15	1	2–15	0.1
			TransMIN charged p_T^{sum}	2–15	1	2–15	0.1
			TransMAX charged p_T^{sum}	2–15	1	2–15	0.1

Table 2: The MPI and CR parameter ranges used in the tuning procedure.

PYTHIA 8 parameter	Min–Max
MPI parameters	
`MultipartonInteractions:pT0Ref`	1.0—3.0
`MultipartonInteractions:ecmPow`	0.0—0.3
`MultipartonInteractions:coreRadius`	0.2—0.8
`MultipartonInteractions:coreFraction`	0.2—0.8
QCD-inspired model	
`ColourReconnection:m0`	0.1—4.0
`ColourReconnection:junctionCorrection`	0.01—10
`ColourReconnection:timeDilationPar`	0—60
Gluon-move model	
`ColourReconnection:m2lambda`	0.2—8.0
`ColourReconnection:fracGluon`	0.8—1.0

$p_{\mathrm{T}}^{\mathrm{sum}}$ as functions of the leading charged particle transverse momentum $p_{\mathrm{T}}^{\mathrm{max}}$, measured in the transMIN and transMAX regions by the CMS experiment at $\sqrt{s} = 13\,\mathrm{TeV}$ [12] and 7 TeV [14] and by the CDF experiment at 1.96 TeV [16]. The N_{ch} as a function of η, measured by CMS at $\sqrt{s} = 13\,\mathrm{TeV}$ [20] is also used in the fit. As for CP5, the region with $p_{\mathrm{T}}^{\mathrm{max}}$ between 0.5 and 2.0 or 3.0 GeV is excluded depending on the distribution from the fit, since it is affected by diffractive processes whose free parameters are not considered in the tuning procedure.

The MPI-related parameters that are kept free in both the CP5-CR1 and CP5-CR2 tunes are:

- `MultipartonInteractions:pT0Ref`, the parameter included in the regularisation of the partonic QCD cross section as described in Eq.(1). It sets the lower cutoff scale for MPIs;
- `MultipartonInteractions:ecmPow`, the exponent of the $\sqrt{s}$ dependence as shown in Eq.(1);
- `MultipartonInteractions:coreRadius`, the width of the core when a double-Gaussian matter profile is assumed for the overlap distribution between the two colliding protons. A double-Gaussian form identifies an inner, dense part, which is called core, and an outer, less dense part;
- `MultipartonInteractions:coreFraction`, the fraction of quarks and gluons contained in the core when a double-Gaussian matter profile is assumed.

The tunable CR parameters in CP5-CR1 that are considered in the fit are:

- `ColourReconnection:m0`, the variable that determines whether a possible reconnection is actually favoured in the λ measure in Eq.(3);
- `ColourReconnection:junctionCorrection`, the multiplicative correction for junction formation, applied to the `m0` parameter;
- `ColourReconnection:timeDilationPar`, the parameter controlling the time dilation that forbids colour reconnection between strings that are not in causal contact.

More details on these parameters are reported in Ref. [1]. For the CP5-CR1 tune, the parameters related to the hadronisation, `StringZ:aLund`, `StringZ:bLund`, `StringFlav:probQQtoQ`, and `StringFlav:probStoUD`, proposed in Ref. [8], are also used as fixed inputs to the tune. The first two of these parameters govern the longitudinal fragmentation function used in the Lund string model in PYTHIA 8, whereas the latter two are the probability of diquark over quark fragmentation, and the ratio of strange to light quark production, respectively.

For the optimisation of CP5-CR2, the following parameters are considered:

- `ColourReconnection:m2lambda`, an approximate hadronic mass-square scale and the parameter used in the calculation of λ;
- `ColourReconnection:fracGluon`, the probability that a given gluon will be moved. It thus gives the average fraction of gluons being considered.

The hadronisation parameters are kept the same as in the CP5 tune, which uses default Monash parameters [25].

The fits are performed using the PROFESSOR 1.4.0 software, which takes random values for each parameter in the defined multidimensional parameter space, and RIVET, which provides the data points and uncertainties, and produces the individual generator predictions for the considered observables. About 200 different choices of parameters are considered to build

a random grid in the parameter space. For each choice of parameters, pp inelastic scattering events, including contributions from single-diffractive dissociation (SD), double-diffractive dissociation (DD), central diffraction (CD), and nondiffractive (ND) processes, are generated. The bin-by-bin envelopes of the different MC predictions are checked. After building the grid in the parameter space, PROFESSOR performs an interpolation of the bin values for the observables in the parameter space using a third-order polynomial function. We verified that the degree of the polynomial used for the interpolation does not affect the tune results significantly. The function $f^b(\mathbf{p})$ models the MC response of each bin b of the observable O as a function of the parameter vector $\mathbf{p}$. The final step is the minimisation of the χ^{*2} function given by:

$$\chi^{*2}(\mathbf{p}) = \sum_O \sum_{b \in O} \frac{(f^b(\mathbf{p}) - \mathcal{R}_b)^2}{\Delta_b^2}, \tag{4}$$

where $\mathcal{R}_b$ is the data value for each bin b, and Δ_b^2 expresses the total bin uncertainty of the data.

The χ^{*2} is not a true χ^2 function as explained in the following. Treating equally all distributions that are used as inputs to the fit for the CP5-CR2 tune results in a tune that describes the data poorly; in particular, it underestimates the $\mathrm{d}N_{\mathrm{ch}}/\mathrm{d}\eta$ distribution measured in data at $\sqrt{s} = 13\,\mathrm{TeV}$ by about 30%. This is because the χ^2 definition treats all bins equally and the importance of $\mathrm{d}N_{\mathrm{ch}}/\mathrm{d}\eta$ may be lost because of its relatively low precision with respect to other observables. The $\mathrm{d}N_{\mathrm{ch}}/\mathrm{d}\eta$ distribution is one of the key observables that is sensitive to a number of processes and, therefore, increasing the importance of this observable in the fit is reasonable.

In PROFESSOR, this is done by using weights with a nonstandard χ^2 definition. To keep the standard properties of a χ^2 fit, we increase the total uncertainties of the other distributions. The total uncertainty in each bin is scaled up by $1/\sqrt{R}$ with R (relative importance) values displayed in Table 1. Therefore, the total uncertainty of each bin of $p_{\mathrm{T}}^{\mathrm{sum}}$ in the transMIN and transMAX regions at $\sqrt{s} = 13\,\mathrm{TeV}$ is scaled up by $\sqrt{2}$ and that of all other distributions by $\sqrt{10}$. These scale factors ensure that the distributions are well described after the tuning. No scaling is needed for the input distributions to the fit for the CP5-CR1 tune, which means that all distributions are considered with the same importance.

The experimental uncertainties used in the fit, in general, have bin-to-bin correlations. However, some of the bins of the UE distributions used in the fit, e.g. $p_{\mathrm{T}}^{\mathrm{max}} > 10\,\mathrm{GeV}$, are dominated by statistical uncertainties, which are uncorrelated between bins. In the minimisation procedure, because the correlations between bins are not available for the input measurements, the experimental uncertainties are assumed to be uncorrelated between data points.

The parameters obtained from the CP5-CR1 and CP5-CR2 fits, as well as the value of the goodness of the fit are shown in Table 3. The uncertainties in the values obtained for the fitted parameters are negligible. In Ref. [10], the number of degrees of freedom for the tune CP5 is given as 63. However, this value of N_{dof} corresponds to the case when only 13 TeV distributions are used. The value of N_{dof} for CP5 consistent with our calculation in this paper is 183.

A preliminary version of the CP5-CR2 tune was derived including several jet substructure observables [26–28] in the fits. This tune, called CP5-CR2-j, has been used in the MC production in the CMS experiment. The CP5-CR2 and CP5-CR2-j tunes have very similar predictions in all final states discussed in this paper, because the tunes differ slightly only in the following parameters, where the listed values are for CP5-CR2-j:

- `MultipartonInteractions:ecmPow` = 0.056,
- `MultipartonInteractions:coreRadius` = 0.653,

Table 3: The parameters obtained in the fits of the CP5-CR1 and CP5-CR2 tunes, compared with that of the CP5 tune. The upper part of the table displays the fixed input parameters of the tune, whereas the lower part shows the fitted tune parameters. The number of degrees of freedom (N_{dof}) and the goodness of fit divided by N_{dof} are also shown.

PYTHIA 8 parameter	CP5 [10]	CP5-CR1	CP5-CR2
PDF set	NNPDF3.1 NNLO	NNPDF3.1 NNLO	NNPDF3.1 NNLO
$\alpha_{\mathrm{S}}(m_{\mathrm{Z}})$	0.118	0.118	0.118
`SpaceShower:rapidityOrder`	on	on	on
`MultipartonInteractions:ecmRef` [GeV]	7000	7000	7000
$\alpha_{\mathrm{S}}^{\mathrm{ISR}}(m_{\mathrm{Z}})$ value/order	0.118/NLO	0.118/NLO	0.118/NLO
$\alpha_{\mathrm{S}}^{\mathrm{FSR}}(m_{\mathrm{Z}})$ value/order	0.118/NLO	0.118/NLO	0.118/NLO
$\alpha_{\mathrm{S}}^{\mathrm{MPI}}(m_{\mathrm{Z}})$ value/order	0.118/NLO	0.118/NLO	0.118/NLO
$\alpha_{\mathrm{S}}^{\mathrm{ME}}(m_{\mathrm{Z}})$ value/order	0.118/NLO	0.118/NLO	0.118/NLO
`StringZ:aLund`	—	0.38	—
`StringZ:bLund`	—	0.64	—
`StringFlav:probQQtoQ`	—	0.078	—
`StringFlav:probStoUD`	—	0.2	—
`SigmaTotal:zeroAXB`	off	off	off
`BeamRemnants:remnantMode`	—	1	—
`ColourReconnection:mode`	—	1	2
`MultipartonInteractions:pT0Ref` [GeV]	1.410	1.375	1.454
`MultipartonInteractions:ecmPow`	0.033	0.033	0.054
`MultipartonInteractions:coreRadius`	0.763	0.605	0.649
`MultipartonInteractions:coreFraction`	0.630	0.445	0.489
`ColourReconnection:range`	5.176	—	—
`ColourReconnection:junctionCorrection`	—	0.238	—
`ColourReconnection:timeDilationPar`	—	8.580	—
`ColourReconnection:m0`	—	1.721	—
`ColourReconnection:m2lambda`	—	—	4.917
`ColourReconnection:fracGluon`	—	—	0.993
N_{dof}	183	157	158
$\chi^{*2}/N_{\mathrm{dof}}$	1.04	2.37	0.89

- MultipartonInteractions:coreFraction = 0.439,
- ColourReconnection:m2lambda = 4.395,
- MultipartonInteractions:fracGluon = 0.990.

The CP1 and CP2 are the two tunes in the CPX (X = 1–5) tune family [10] that use an LO PDF set [24]. We also derive CR tunes based on the CP1 and CP2 settings to study the effect of using a leading order (LO) PDF set with alternative CR models, although they are not used in precision measurements. We find that the predictions of the CR tunes based on CP1 and CP2 for the MB and UE observables are similar to the prediction of CR tunes based on CP5. However, CP1-CR1 (i.e. CP1 with the QCD-inspired colour reconnection model) has a different trend in particle multiplicity distributions compared with the predictions of other tunes discussed in this study. This different trend of CP1-CR1 cannot be attributed to the use of LO PDF set, because both CP1 and CP2 use the same LO PDF set and we do not see a different trend with CP2-CR1. The trend observed with CP1-CR1 in the particle multiplicity distributions could be an input for further tuning and development of the QCD-inspired model. Therefore, in Appendix A of this paper, we present the tune settings of the CR tunes based on CP1 and CP2, along with their predictions in the particle multiplicity distributions.

4 Performance of the tunes

In Figs. 5–18 we show the observables measured at centre-of-mass energies of 1.96, 7, 8, and 13 TeV. The CMS data points are shown in black, and are compared with simulations obtained from the PYTHIA 8 event generator with the tunes CP5 (red), CP5-CR1 (blue), and CP5-CR2 (green). For simplicity, the tunes CP5-CR1 and CP5-CR2 will be referred to as CP5-CR when convenient. The lower panels show the ratios between each MC prediction and the data.

4.1 Underlying-event and minimum-bias observables

"Minimum bias" is a generic term used to describe events collected with a loose selection process that are dominated by relatively soft particles. Although these events generally correspond to inelastic scattering, including ND and SD+DD+CD processes, these contributions may vary depending on the trigger requirements used in the experiments. For example, a sample of non-single-diffractive-enhanced (NSD-enhanced) events is selected by suppressing the SD contribution at the trigger level. For all of the plots presented in this section, inelastic events (i.e. ND, SD, DD, and CD) are simulated with PYTHIA 8.226 and compared with data at different centre-of-mass energies. The rest of the plots are produced with PYTHIA 8.235. An update to the description of the elastic scattering component in PYTHIA 8.235 led to a slight decrease in the default ND cross section. The default ND cross section in PYTHIA 8.226, which is 55.51 mb at $\sqrt{s} = 13$ TeV, is lowered to 55.14 mb in PYTHIA 8.235. Hence, to reproduce the conditions of PYTHIA 8.226 in PYTHIA 8.235 or in a newer version, one should set the ND cross section manually.

The UE observables measured by the CMS experiment at $\sqrt{s} = 13$ TeV [12], namely N_{ch} density and the average $p_{\mathrm{T}}^{\mathrm{sum}}$ in the transMIN and transMAX regions are well described by all tunes in the plateau region as shown in Fig. 5. The region up to $\approx$5 GeV of $p_{\mathrm{T}}^{\mathrm{max}}$ is highly sensitive to diffractive contributions [29]. There is a lack of measurements in this region where the tunes, in general, do not perform well. Although the optimisation of these components is beyond the scope of this study, we have extended the fit range to $\approx$2–3 GeV as long as the data are well described. The rising part of the spectrum excluding the region up to $\approx$5 GeV of the N_{ch} density distributions is similarly described by all tunes, whereas in the $p_{\mathrm{T}}^{\mathrm{sum}}$ density distributions the

predictions of CP5 differ slightly from the predictions of the CR tunes. These show that the CP5 tune has a harder p_{T} spectrum at low $p_{\mathrm{T}}^{\mathrm{max}}$ values. In Fig. 6 observables sensitive to the softer part of the MPI spectrum, such as the pseudorapidity distribution of charged hadrons in inelastic pp collisions measured by the CMS experiment at $\sqrt{s} = 13\,\mathrm{TeV}$ [20] are well described by all tunes.

A crucial test for the performance of UE tunes, and of the CR simulation in particular, is the description of the average p_{T} of the charged particles as a function of N_{ch}. Comparisons of the mean average p_{T} to the measurements by the ATLAS Collaboration at $\sqrt{s} = 13\,\mathrm{TeV}$ in the transMAX and transMIN regions [13] are displayed in Fig. 7. The tune CP5 describes the central values of the data perfectly for $N_{\mathrm{ch}} > 7$, whereas the CR tunes show an almost constant discrepancy of 5–10% because of the harder p_{T} spectrum predicted by the tune CP5 for low-p_{T} particles. All CR tunes show a reasonable agreement with the data, confirming the accuracy of the parameters obtained for the new CR models. The improvement in the tuned CR models and their success in describing the data is seen by comparing Fig. 5 with Fig. 3, and Fig. 6 with Fig. 4.

In Fig. 8, charged-particle and $p_{\mathrm{T}}^{\mathrm{sum}}$ densities measured by the CMS experiment at $\sqrt{s} = 7\,\mathrm{TeV}$ [14] in the transMIN and transMAX regions, as functions of the leading charged particle p_{T}, $p_{\mathrm{T}}^{\mathrm{max}}$, are compared with predictions from the tunes CP5 and CP5-CR. The data are reasonably well described for $p_{\mathrm{T}}^{\mathrm{max}} > 5\,\mathrm{GeV}$.

In Fig. 9, charged particle and $p_{\mathrm{T}}^{\mathrm{sum}}$ densities in the transverse region, as functions of the leading charged particle p_{T}, and the average p_{T} in the transverse region as functions of the leading charged particle p_{T} and of the N_{ch}, measured by the ATLAS experiment at $\sqrt{s} = 7\,\mathrm{TeV}$ [15], are compared with the predictions from the tunes CP5 and CP5-CR. The central values of the average p_{T} in bins of the leading charged particle p_{T} and of the N_{ch} are consistent with the data points within 10%. A similar level of agreement as observed at 13 TeV is achieved by the new tunes at 7 TeV.

The performance of the new tunes is also checked at 7 TeV using inclusive measurements of charged-particle pseudorapidity distributions. In Fig. 10, the CMS measurements for $\mathrm{d}N_{\mathrm{ch}}/\mathrm{d}\eta$ at 7 TeV [30] with at least one charged particle in $|\eta| < 2.4$ are compared with predictions from the tunes CP5 and CP5-CR. The CP5 and CP5-CR1 have similar predictions, while CP5-CR2 predicts about 4% less charged particles than the first two tunes in all η bins of the measurement. Although all tunes provide a reasonable description of $\mathrm{d}N_{\mathrm{ch}}/\mathrm{d}\eta$ with deviations up to $\approx$10%, the data and MC simulation show different trends for $|\eta| > 1.2$, where the trend for the data is not described well by the tunes. In the more central region, i.e. $|\eta| < 1.2$, the shape of the predictions agrees well with the data but there is a difference in normalisation. For example, CP5 and CP5-CR1 predict 3–4% and CP5-CR2 predicts about 7% fewer charged particles in all bins for $|\eta| < 1.2$ compared with the data.

In Fig. 11, charged-particle and $p_{\mathrm{T}}^{\mathrm{sum}}$ densities measured as functions of the p_{T} of the leading charged particle at $\sqrt{s} = 1.96\,\mathrm{TeV}$ by the CDF experiment [16] in the transMIN and transMAX regions are compared with predictions from the tunes CP5 and CP5-CR, respectively. All predictions reproduce the UE observables within $\approx$10% at $\sqrt{s} = 1.96$, 7, and 13 TeV.

We compare the new CMS tunes also with MB and UE data measured at forward pseudorapidities. The energy density, $\mathrm{d}E/\mathrm{d}\eta$, measured in MB events and in NSD events by the CMS experiment at $\sqrt{s} = 13\,\mathrm{TeV}$, is shown in Fig. 12. The data are well described by CP5-CR2 within uncertainties and for all measured $|\eta|$ bins. The predictions of CP5 and CP5-CR1 overestimate the data in $4.2 < |\eta| < 4.9$.

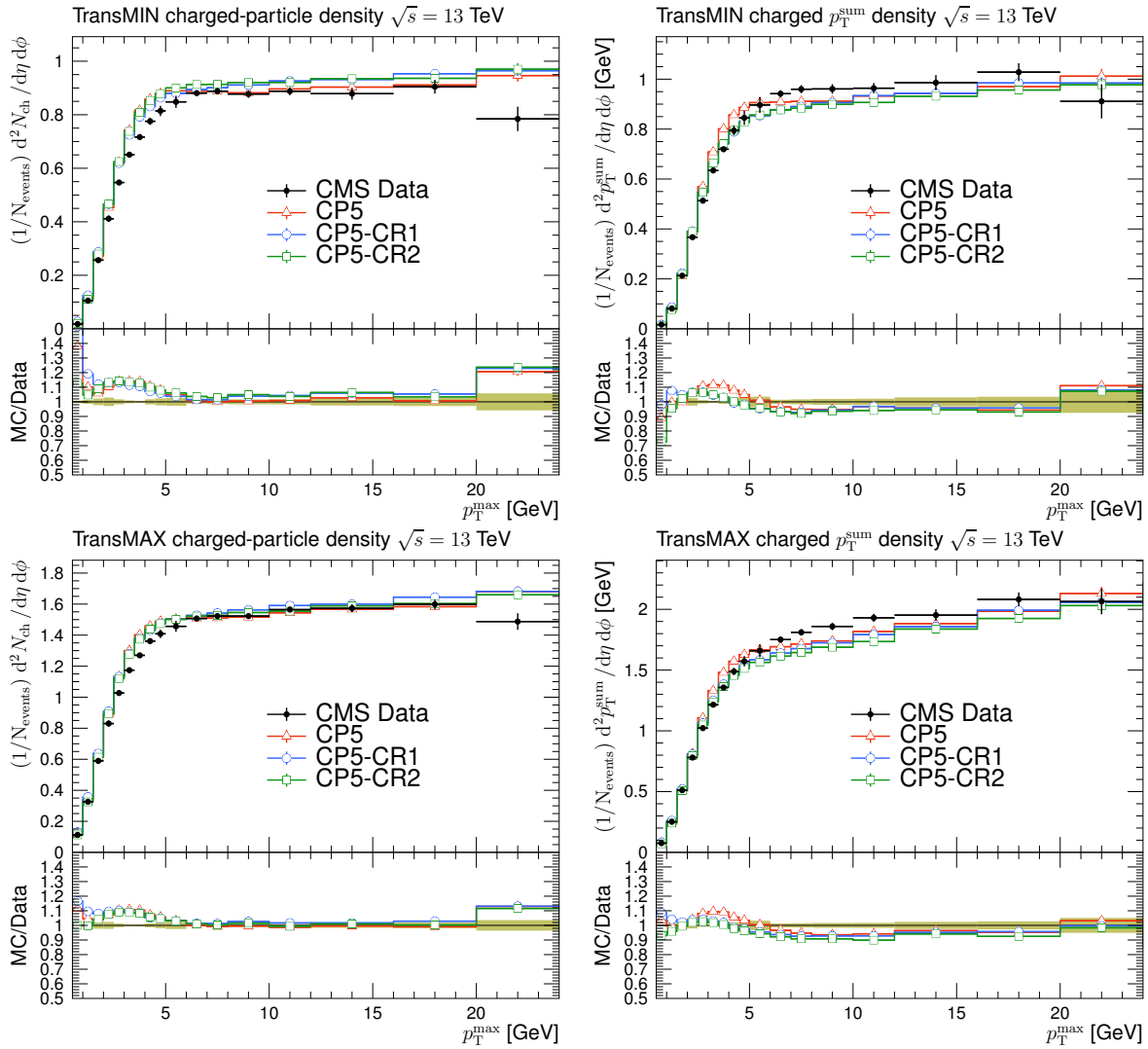

Figure 5: The charged-particle (left) and $p_{\mathrm{T}}^{\mathrm{sum}}$ (right) densities in the transMIN (upper) and transMAX (lower) regions, as functions of the p_{T} of the leading charged particle, $p_{\mathrm{T}}^{\mathrm{max}}$, measured by the CMS experiment at $\sqrt{s} = 13\,\mathrm{TeV}$ [12]. The predictions of the CP5 and CP5-CR tunes are compared with data. The coloured band and error bars on the data points represent the total experimental uncertainty in the data.

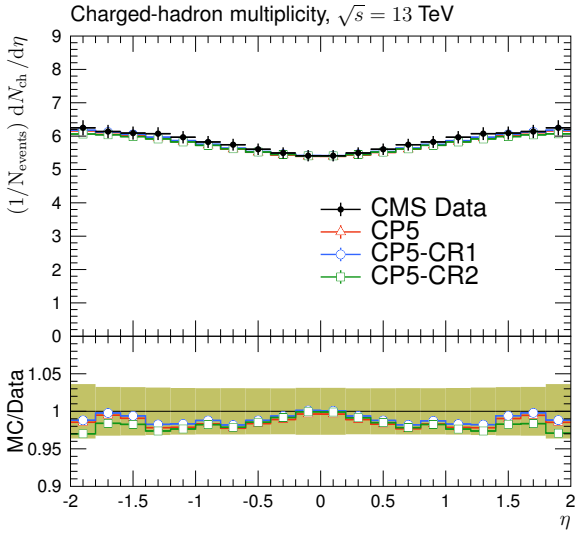

Figure 6: The pseudorapidity of charged hadrons, $\mathrm{d}N_{\mathrm{ch}}/\mathrm{d}\eta$, measured by the CMS experiment at $\sqrt{s} = 13$ TeV [20]. The predictions of the CP5 and CP5-CR tunes are compared with data. The coloured band and error bars on the data points represent the total experimental uncertainty in the data.

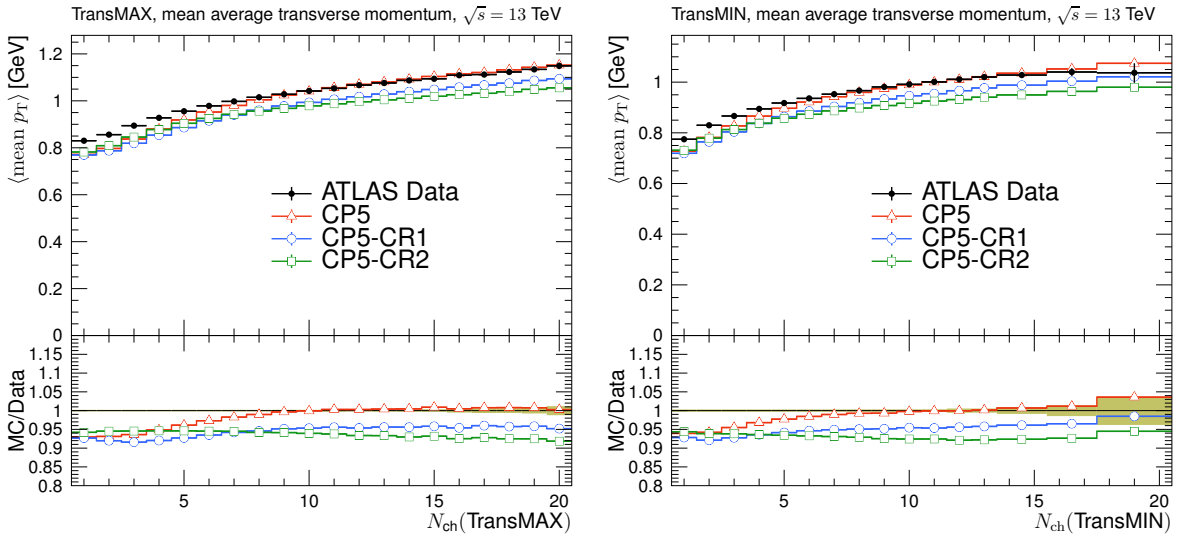

Figure 7: The mean charged-particle average transverse momentum as functions of charged-particle multiplicity in the transMAX (upper) and transMIN (lower) regions, measured by the ATLAS experiment at $\sqrt{s} = 13$ TeV [13]. The predictions of the CP5 and CP5-CR tunes are compared with data. The coloured band and error bars on the data points represent the total experimental uncertainty in the data.

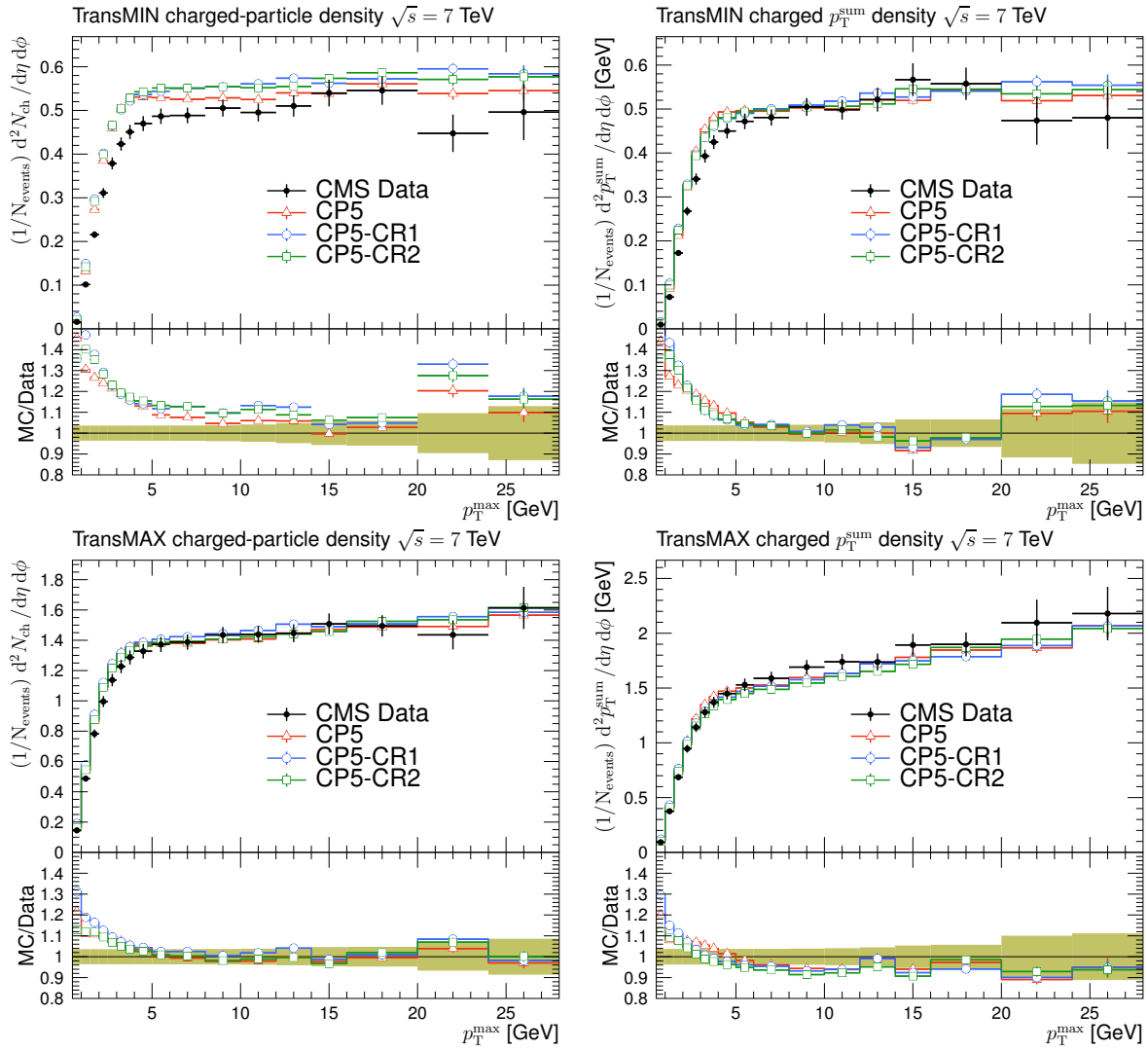

Figure 8: The charged-particle (left) and $p_{\mathrm{T}}^{\mathrm{sum}}$ (right) densities in the transMIN (upper) and transMAX (lower) regions, as functions of the p_{T} of the leading charged particle, $p_{\mathrm{T}}^{\mathrm{max}}$, measured by the CMS experiment at $\sqrt{s} = 7\,\mathrm{TeV}$ [14]. The predictions of the CP5 and CP5-CR tunes are compared with data. The coloured band and error bars on the data points represent the total experimental uncertainty in the data.

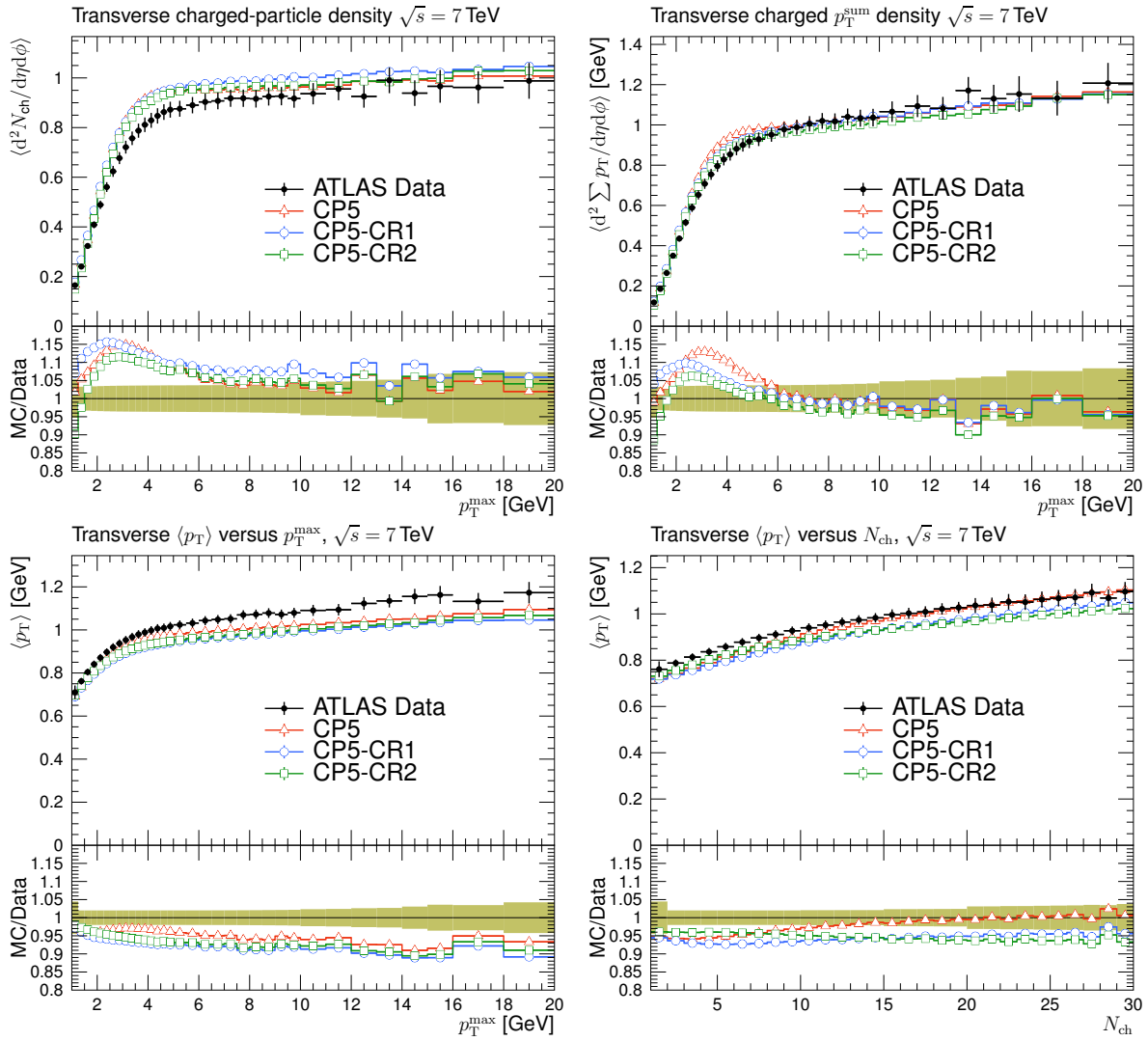

Figure 9: The charged-particle (upper left) and p_T^{sum} densities (upper right) in the transverse region, as functions of the p_T of the leading charged particle, and average transverse momentum in the transverse region as functions of the leading charged particle p_T (lower left) and of the charged particle multiplicity (lower right), measured by the ATLAS experiment at $\sqrt{s} = 7$ TeV [15]. The predictions of the CP5 and CP5-CR tunes are compared with data. The coloured band and error bars on the data points represent the total experimental uncertainty in the data.

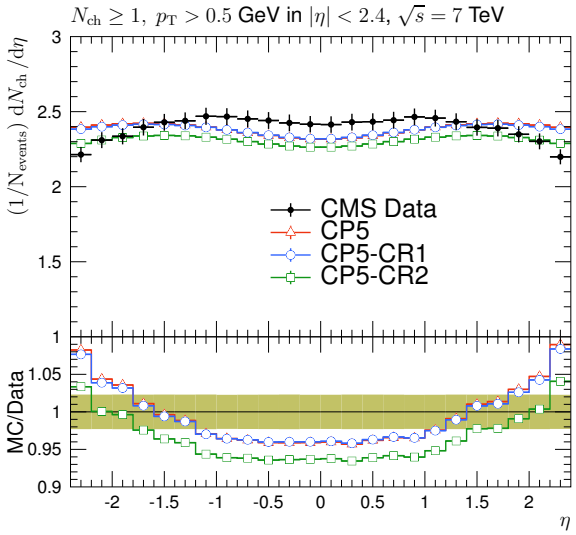

Figure 10: The pseudorapidity of charged particles, $\mathrm{d}N_{\mathrm{ch}}/\mathrm{d}\eta$, with at least one charged particle in $|\eta| < 2.4$, measured by the CMS experiment at $\sqrt{s} = 7$ TeV [30]. The predictions of the CP5 and CP5-CR tunes are compared with data. The coloured band and error bars on the data points represent the total experimental uncertainty in the data.

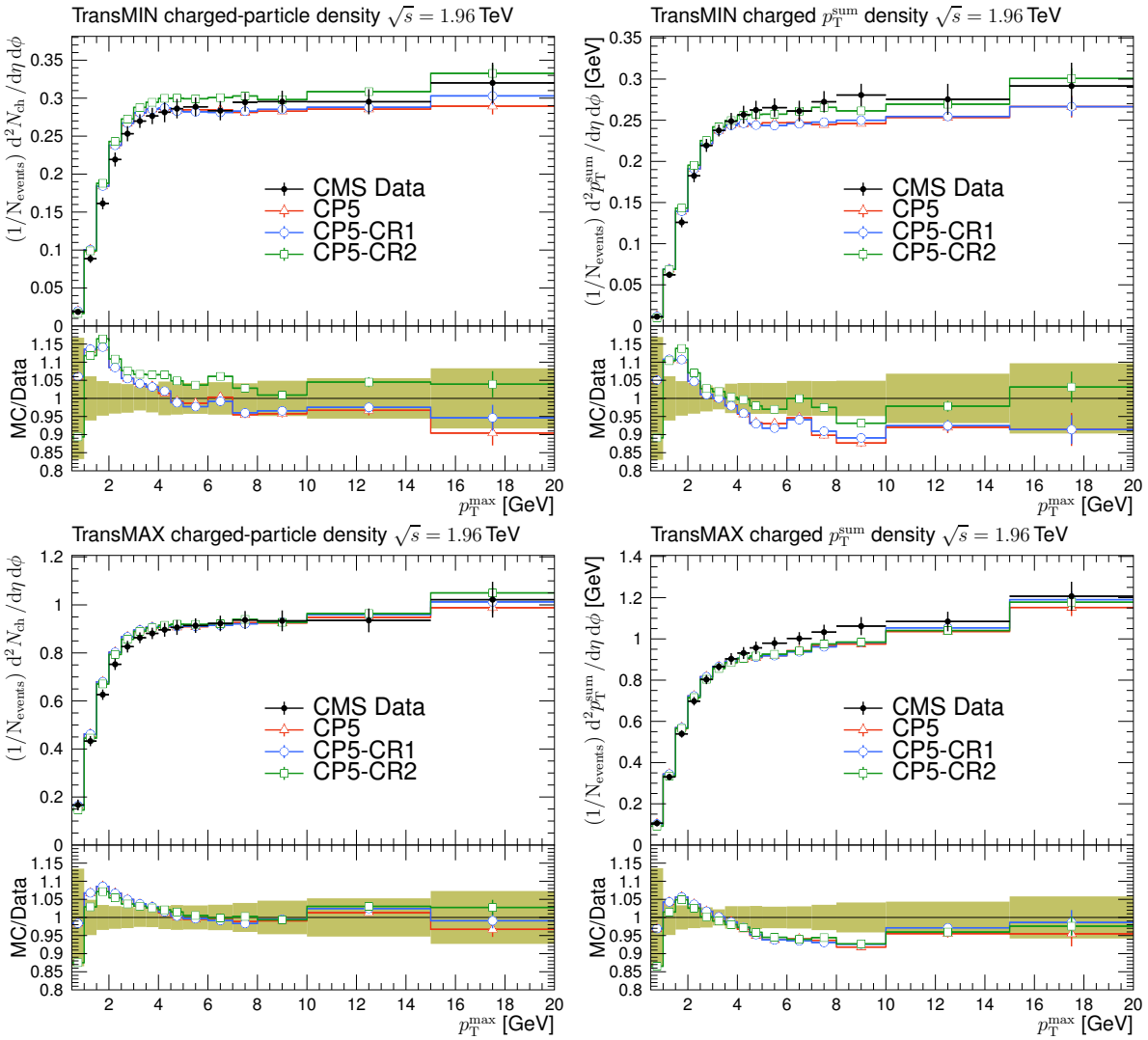

Figure 11: The charged-particle (left) and $p_{\mathrm{T}}^{\mathrm{sum}}$ densities (right) in the transMIN (upper) and transMAX (lower) regions, as functions of the p_{T} of the leading charged particle, $p_{\mathrm{T}}^{\mathrm{max}}$, measured by the CDF experiment at $\sqrt{s} = 1.96\,\mathrm{TeV}$ [16]. The predictions of the CP5 and CP5-CR tunes are compared with data. The coloured band and error bars on the data points represent the total experimental uncertainty in the data.

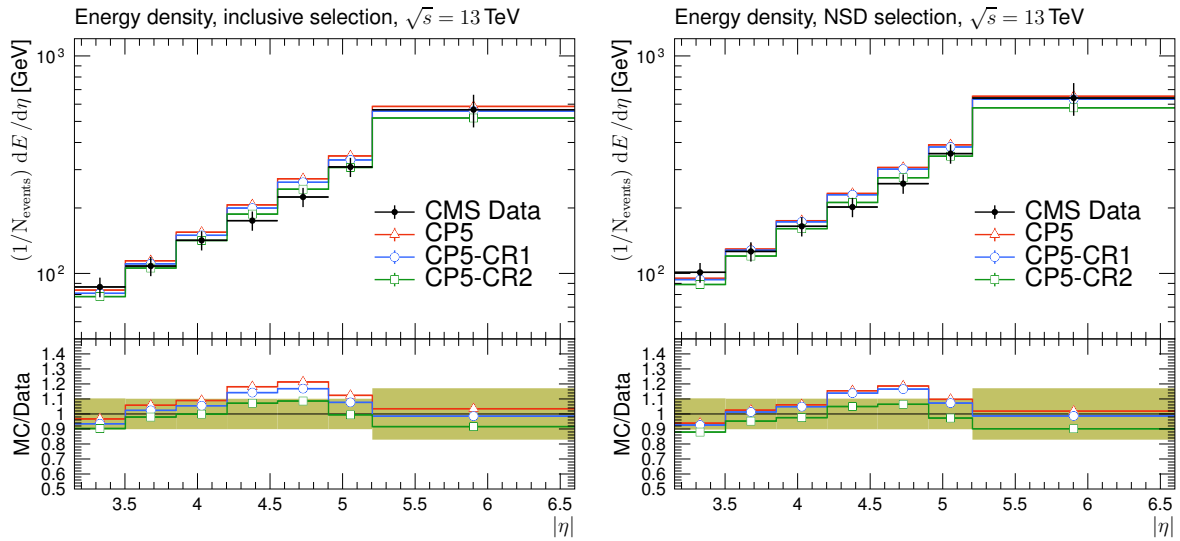

Figure 12: The energy density as a function of pseudorapidity, in two different selections, in MB events (left) and in events with a presence of a hard dijet system (right), measured by the CMS experiment at $\sqrt{s} = 13$ TeV [31]. The predictions of the CP5 and CP5-CR tunes are compared with data. The coloured band and error bars on the data points represent the total experimental uncertainty in the data.

4.2 Particle multiplicities

Figure 13 shows the strange particle production for Λ baryons and K^0_S mesons as a function of rapidity measured by the CMS experiment [32] in NSD events at $\sqrt{s} = 7\,\text{TeV}$. The NSD events are simulated with PYTHIA 8.226, and the predictions of the tunes are compared with data as shown in the figure. We show in Ref. [8] that the new CR models might be beneficial for describing the ratios of strange particle multiplicities, for example Λ/K^0_S in pp collisions. We observe that all CP5 tunes, regardless of the CR model, describe particle production for K^0_S mesons as a function of rapidity very well. However, they underestimate particle production for Λ versus rapidity by about 30%. Therefore, the ratio Λ/K^0_S is not perfectly described but this could be improved by different hadronisation models [33, 34].

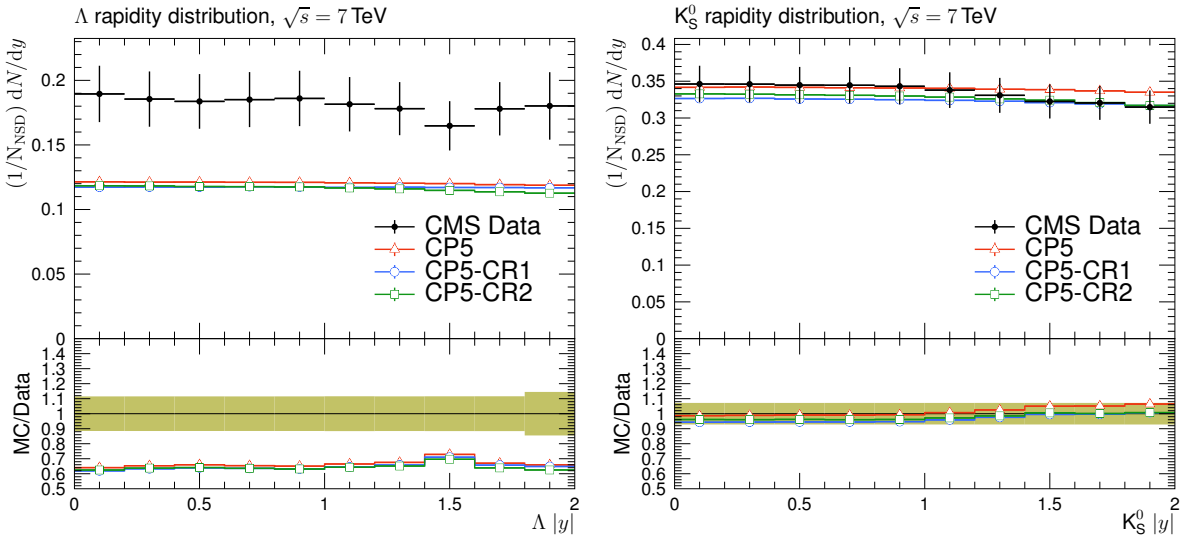

Figure 13: The strange particle production, Λ baryons (left) and K^0_S mesons (right), as a function of rapidity, measured by the CMS experiment at $\sqrt{s} = 7\,\text{TeV}$ [32]. The predictions of the CP5 and CP5-CR tunes are compared with data. The coloured band and error bars on the data points represent the total experimental uncertainty in the data.

The multiplicities of identified particles are also investigated in simulated MB events (ND+SD+DD+CD). Figure 14 shows the ratio of proton over pion production, as a function of particle p_T [35]. All the tunes predict a similar trend, showing that the new CR models do not lead to a significant improvement in the description of the ratio of proton to pion production. However, it is known that this observable is strongly correlated with event particle multiplicity [35–37] and not only CR, since also hadronisation and MPI play a key role in describing the ratios of particle yields. The ratios of all light, charm, and bottom baryons to mesons are shown in Fig. 15, together with data from charm factories [38, 39]. This is one of the key observables to correctly obtain the identified-particle spectra. Although there is no data for the yield ratio of light baryons to mesons, the predictions of the models are compared with each other, which can provide valuable information for further tuning of these models. The tunes provide a good description of the baryon-to-meson yield ratios at different centre-of-mass energies.

4.3 Jet substructure observables

The number of charged particles contained in jets is an important observable that makes it possible to distinguish quark-initiated jets from gluon-initiated jets. The average number of charged hadrons with $p_T > 500\,\text{MeV}$ inside the jets measured by the CMS experiment as a function of the jet p_T is shown in Fig. 16 [26]. The predictions of the CR tunes are comparable,

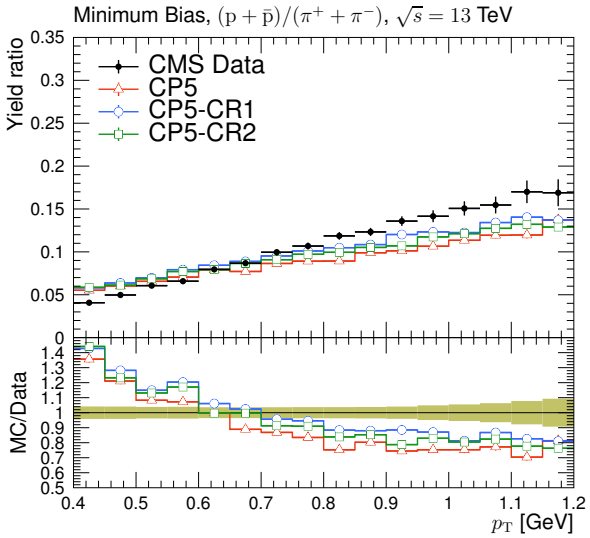

Figure 14: Ratios of particle yields, p/π, as a function of transverse momentum in mininum-bias events, measured by the CMS experiment at $\sqrt{s} = 13$ TeV [35]. The predictions of the CP5 and CP5-CR tunes are compared with CMS data. The coloured band and error bars on the data points represent the total experimental uncertainty in the data.

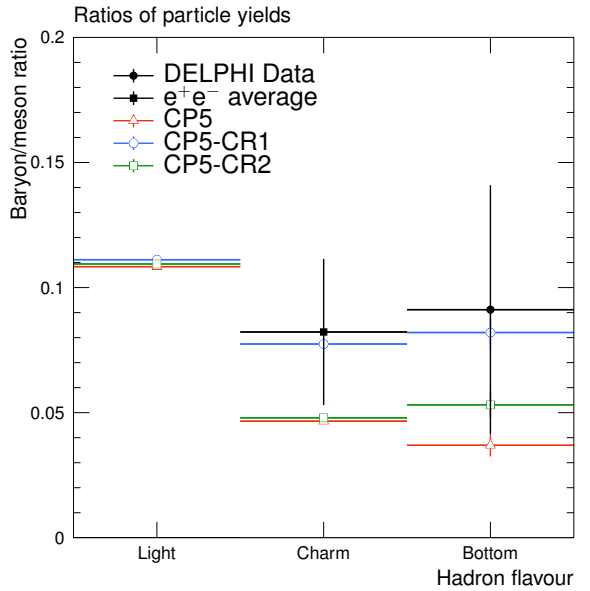

Figure 15: Ratios of particle yields for light, charm, and bottom hadrons predicted by the CP5 and CP5-CR tunes compared with data from e^+e^- colliders [38, 39]. The error bars on the data points represent the total experimental uncertainty in the data.

and produce roughly 5% fewer charged particles than the CP5 tune. All predictions show a reasonable description of the data.

Figure 17 presents the distributions of $F(z) = (1/N_{\text{jet}})(\mathrm{d}N_{\text{ch}}/\mathrm{d}z)$, where z is the longitudinal momentum fraction, and N_{ch} is the charged-particle multiplicity in the jet, measured by the ATLAS experiment at $\sqrt{s} = 7\,\text{TeV}$ [27]. The $F(z)$ parameter is related to the fragmentation function and is presented for $p_{\text{T}}^{\text{jet}} = 25\text{–}40\,\text{GeV}$ and $p_{\text{T}}^{\text{jet}} = 400\text{–}500\,\text{GeV}$. The CR tunes describe low-$p_{\text{T}}^{\text{jet}}$ data better than CP5, and their predictions reasonably agree with the high-$p_{\text{T}}^{\text{jet}}$ data, except for the last bin. The high-$p_{\text{T}}^{\text{jet}}$ data are well described by the CP5 tune within the uncertainties, and its central values agree better with the predictions of the CP5 tune than with those of the CP5-CR tunes.

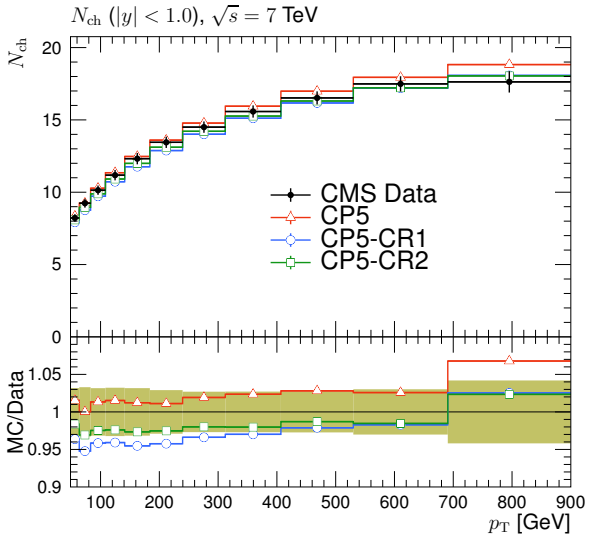

Figure 16: Average charged-hadron multiplicity, as a function of the jet p_{T}, for jets with rapidity $|y| < 1$, measured by the CMS experiment at $\sqrt{s} = 7\,\text{TeV}$ [26]. The predictions of the CP5 and CP5-CR tunes are compared with data. The coloured band and error bars on the data points represent the total experimental uncertainty in the data.

4.4 Drell–Yan events

Drell–Yan (DY) events with the Z boson decaying to $\mu^+\mu^-$ were generated with PYTHIA 8 and compared with CMS data at $\sqrt{s} = 13\,\text{TeV}$. Figure 18 shows the N_{ch} and p_{T} flow as a function of the Z boson p_{T} (in the invariant $\mu^+\mu^-$ mass window of 81–101 GeV) in the region transverse to the boson momentum [40], which is expected to be dominated by the underlying event.

The CP5 tunes predict up to 15% too many charged particles at low Z boson p_{T}, where additional effects, such as the intrinsic transverse momentum of the interacting partons (i.e. primordial k_{T}) are expected to play a role. Higher-order corrections, as implemented in MADGRAPH5_aMC@NLO v2.4.2 [41] with FxFx merging [42], are necessary to describe the total p_{T} flow. The impact of the different CR models is negligible in DY events.

4.5 Top quark observables

4.5.1 Jet substructure in $\mathrm{t\bar{t}}$ events

A study of the UE in $\mathrm{t\bar{t}}$ events [18] also estimated the effects of the CR on the top quark decay products by investigating the differences between predictions using PYTHIA 8 with the

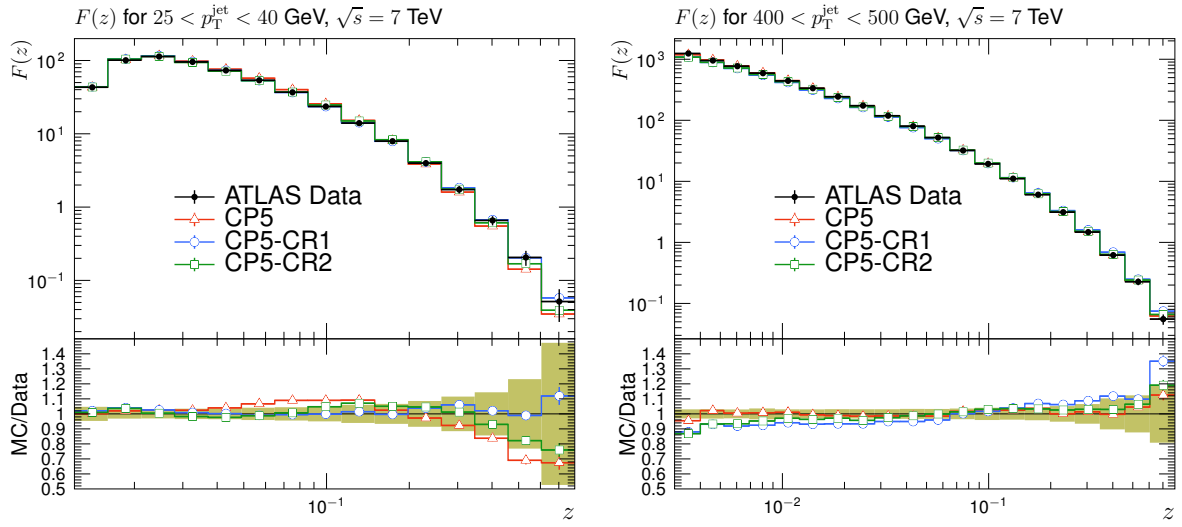

Figure 17: Distributions of $F(z)$ for $25 < p_T^{jet} < 40$ GeV (left) and $400 < p_T^{jet} < 500$ GeV (right) for jets with pseudorapidity $|\eta_{jet}| < 1.2$, measured by the ATLAS experiment at $\sqrt{s} = 7$ TeV [27]. The predictions of the CP5 and CP5-CR tunes are compared with data. The coloured band and error bars on the data points represent the total experimental uncertainty in the data.

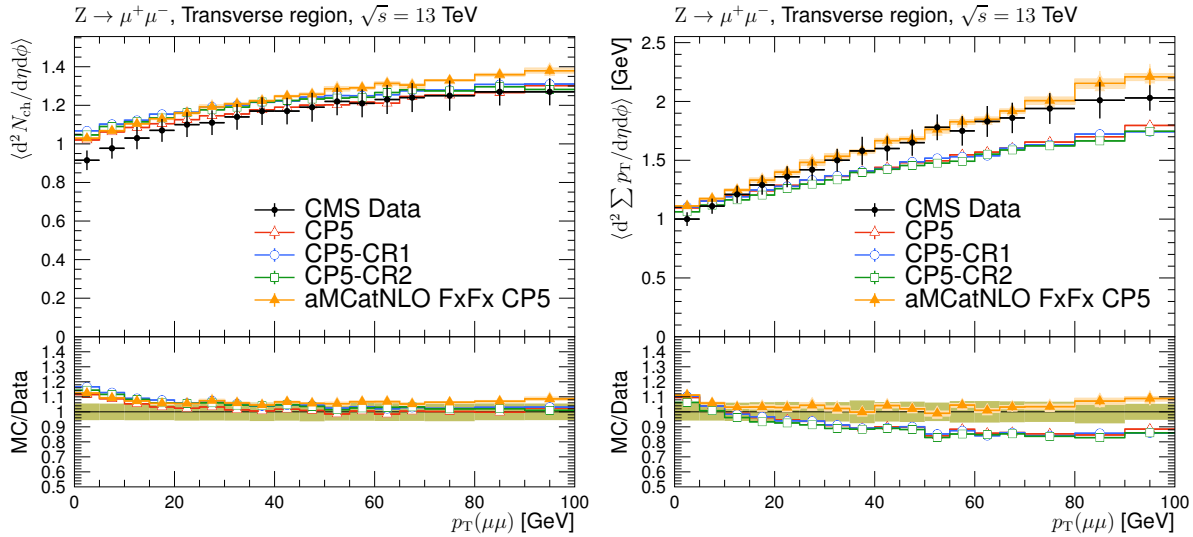

Figure 18: Number of charged particles and p_T flow in the transverse region of DY events, measured by the CMS experiment at $\sqrt{s} = 13$ TeV in bins of Z boson p_T [40]. The plots show the predictions of the CP5 and CP5-CR tunes compared with data. The coloured band and error bars on the data points represent the total experimental uncertainty in the data.

ERD off and on options. In Ref. [18], in addition to the QCD-inspired and gluon-move models, predictions of the rope hadronisation model are also compared with the data. In the rope hadronization model, overlapping strings are treated to act coherently as a "rope". The interactions between overlapping strings are described by an interaction potential inspired by the phenomenology of superconductors [33, 34, 43–48]. The ERD off and on options allow the CR to take place before or after the top quark decay, respectively. In particular, the ERD option allows the top quark decay products to be colour reconnected with the partons from MPI systems. Ref. [18] showed that these different models and options produce similar predictions for UE observables in $t\bar{t}$ events. However, some jet-shape distributions in $t\bar{t}$ events display a more significant effect [49], e.g. in the number of charged particles in jets. In the following, we investigate how the PYTHIA 8 CR tunes describe the CMS $t\bar{t}$ jet substructure data [49]. In the CMS measurement, jets reconstructed using the anti-k_T algorithm [50] with a distance parameter of $R = 0.4$ as implemented in FASTJET 3.1 [51] are used. Jets with $p_T > 30\,\text{GeV}$ within $|\eta| < 2$ are selected. Jet pairs (j_1 and j_2) are required to be far from each other in η-ϕ space, $\Delta R(j_1, j_2) = \sqrt{(\eta_{j_1} - \eta_{j_2})^2 - (\phi_{j_1} - \phi j_2)^2} > 0.8$. Jet substructure observables are calculated from jet constituents with $p_T > 1\,\text{GeV}$, e.g. in the plateau region of high track finding efficiency and low misidentification rate. Here we focus on two variables, (i) $\lambda_0^0(N)$, which is the number of charged particles with $p_T > 1\,\text{GeV}$ in the jet, and (ii) the separation between two groomed subjets, ΔR_g, that are shown in Fig. 19 for gluon jets and inclusive jets, respectively. A "groomed jet" refers to a jet with soft and wide-angle radiation removed by a dedicated grooming algorithm [52, 53].

The compatibility of data and MC predictions is evaluated using a measure defined as $\chi^2 = \Delta^T C^{-1} \Delta$, where Δ is the difference vector between measured and predicted values, and C is the total covariance matrix of the measurement. Since the measured distribution is normalised to unity, its covariance matrix is singular, i.e. not invertible. To render C invertible, the vector entry and matrix row/column corresponding to one measured bin need to be discarded; we choose to remove the last bin. The results are displayed in Table 4 for all jets inclusively as well as for each jet flavour separately. We observe that none of the tunes describe the $\lambda_0^0(N)$ data well for all jet flavours. As concluded in Ref. [49], flavour-dependent improvements in the nonperturbative physics modelling may be required for a better description of the data. The angle between the groomed subjets, on the other hand, is infrared and collinear safe and can be described very well by an increase in the FSR α_s, which corresponds to a decrease in the renormalisation scale.

4.5.2 Pull angle in $t\bar{t}$ events

Figure 20 displays the normalised $t\bar{t}$ differential cross section for the jet pull angle [55] defined using the jets originating from the decay of a W boson in $t\bar{t}$ events, as measured by the ATLAS experiment [54]. The observable is shown for the case where only the charged constituents of the jet are used in the calculation. The data are compared with predictions from POWHEG v2 [56]+PYTHIA 8 using the CP5 tunes or the corresponding CR tunes. The χ^2 values are calculated as described in Section 4.5.1 and are shown in the last column of Table 4. The pull angle is particularly sensitive to the setting of the ERD option. With ERD turned off, the decay products of the W boson in $t\bar{t}$ events are not included in CR, and the predictions using the tunes with the various CR models are similar to each other. With ERD enabled, CR now modifies the pull angle between the two jets, which is observed in Fig. 20. The predictions of each tune also show significant changes when ERD is enabled. For both the nominal and CR1 (QCD-inspired) tunes, the prediction with ERD improves the description of the data, and the difference between the predictions with or without ERD is larger for the CR1-based tune. We

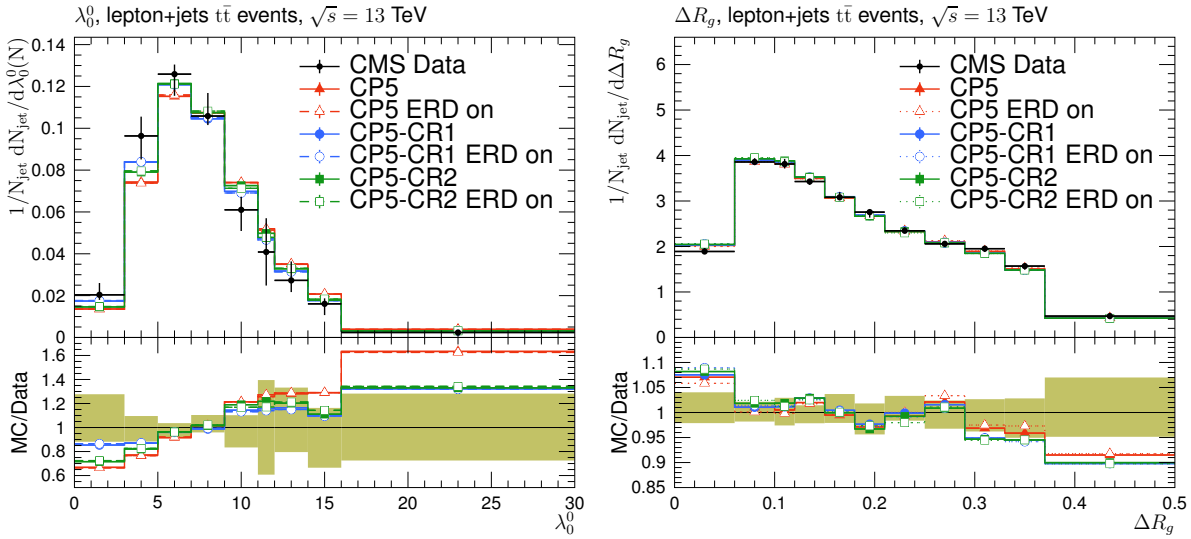

Figure 19: Distributions of the particle multiplicity in gluon jets (upper) and the angle ΔR_g between two groomed subjets in inclusive jets (lower) measured by the CMS experiment in $t\bar{t}$ events at $\sqrt{s} = 13$ TeV [49]. The coloured band and error bars on the data points represent the total experimental uncertainty in the data.

Table 4: The χ^2 values and the numbers of degrees of freedom (N_{dof}) for the comparison of $t\bar{t}$ data with the predictions of the different PYTHIA 8 tunes, for the distributions of the charged-particle multiplicity λ_0^0, the angle between the groomed subjets ΔR_g at $\sqrt{s}$ = 13 TeV [49], and the pull angle measured in the ATLAS analysis of the colour flow at 8 TeV [54]. The FSR up and down entries denote variations of the renormalisation scale in the FSR shower by factors of 0.5 and 2, respectively.

	Charged-particle multiplicity λ_0^0					Angle between groomed subjets ΔR_g					Pull angle $\phi(j_1, j_2)$	
	χ^2				N_{dof}	χ^2				N_{dof}	χ^2	N_{dof}
Tune	Incl.	Bottom	Light	Gluon		Incl.	Bottom	Light	Gluon			
CP5	18.4	26.6	30.7	11.8	8	28.2	18.3	10.6	8.1	10	4.7	3
CP5 ERD	19.6	28.7	32.2	12.2	8	26.9	15.0	10.7	8.7	10	2.4	3
CP5 FSR up	28.4	43.7	33.0	14.6	8	13.3	4.2	5.8	5.7	10	5.9	3
CP5 FSR down	15.0	19.7	44.0	11.6	8	59.6	39.2	33.1	22.6	10	4.1	3
CP5-CR1	14.3	28.4	29.5	4.1	8	34.6	13.4	24.4	23.6	10	3.9	3
CP5-CR1 ERD	11.7	24.4	27.8	3.8	8	32.7	13.4	21.1	27.0	10	1.4	3
CP5-CR2	14.1	23.8	38.3	8.1	8	34.3	22.3	21.3	11.7	10	5.2	3
CP5-CR2 ERD	11.0	16.9	38.6	7.1	8	35.3	24.8	16.1	13.1	10	9.3	3

observe the opposite for the CR2-based (gluon-move) tunes. The choice without ERD is preferred here. This picture might be different if the flip mechanism had been added in the tuning of the gluon-move model. The move step in the gluon-move model is more restrictive because it allows only gluons to move between the string end-points. The inclusion of the flip mechanism would also allow the string end-points to be mixed with each other and, therefore, could further reduce the total string length in an event. However, as indicated earlier, the effect of the flip mechanism on diffractive events is not well understood and, therefore, this mechanism is not used in this paper.

Overall, the QCD-inspired model with ERD provides the best description of the jet pull angle. The differences between the predictions using the different tunes observed here indicate that the inclusion of observables, such as the jet pull angle and other jet substructure observables, could be beneficial in future tune derivations.

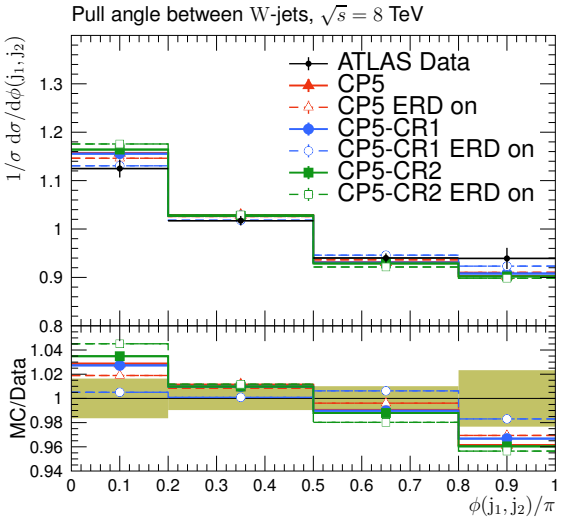

Figure 20: Normalised $\mathrm{t\bar{t}}$ differential cross section for the pull angle between jets from the W boson in top quark decays, calculated from the charged constituents of the jets, measured by the ATLAS experiment using $\sqrt{s} = 8$ TeV data [54] to investigate colour flow. The coloured band and error bars on the data points represent the total experimental uncertainty in the data.

5 Uncertainty in the top quark mass due to colour reconnection

The top quark mass has been measured with high precision using the 7, 8, and 13 TeV $\mathrm{t\bar{t}}$ data at the LHC [19, 57–69]. The most precise value of $m_\mathrm{t} = 172.44 \pm 0.13\,(\mathrm{stat}) \pm 0.47\,(\mathrm{syst})$ GeV was measured by the CMS Collaboration combining 7 and 8 TeV data [63]. To further improve the precision of m_t measurements, a complete analysis of the systematic uncertainties in the measurement is crucial. One of the dominant systematic uncertainties is due to the modelling of CR in top quark decays [63]. The procedure for estimating this uncertainty used for the LHC Run 1 (years 2009–2013) analyses at $\sqrt{s} = 7$ and 8 TeV was based on a comparison of two values of m_t, calculated by using predictions with the same UE tune with and without CR effects. The new CMS tunes, presented in Section 2, which use different CR models, can be used to give a better evaluation of the CR uncertainty. In particular, the uncertainty are now calculated by comparing results for m_t values obtained from different realistic CR models, such as the default model in PYTHIA 8 (MPI-based model) and the other ones, QCD-inspired and gluon-move.

Additionally, one can also estimate the effects of the CR on the top quark decay products by investigating the differences between predictions using PYTHIA 8 with the option ERD off and

on, which was done for the UE observables [18].

A determination of m_t using a kinematic reconstruction of the decay products in semileptonic $t\bar{t}$ events at $\sqrt{s} = 13$ TeV is reported in Ref. [19]. In these events, one of the W bosons from the top quark decays into a muon or electron and a neutrino, and the other into a quark-antiquark pair. In this analysis, m_t and the jet energy scale factor were determined simultaneously through a joint-likelihood fit to the selected events. The results with the QCD-inspired and gluon-move models were also compared. The PYTHIA 8 CUETP8M2T4 [70] UE tune was used, and the parameters of the CR models were tuned to UE and MB data at $\sqrt{s} = 13$ TeV [19]. They found that the gluon-move model results in a larger shift in the m_t value of 0.31 GeV, which was assumed as the uncertainty due to the modelling of CR in the measured m_t. This is the largest source of uncertainty in the measured m_t, where the total uncertainty is 0.62 GeV. Similar studies using single top quark final states are reported in Refs. [67, 71].

We compare the m_t and W boson mass values obtained with different tune configurations based on our new tunes in Table 5. Top quark candidates are constructed by a RIVET routine in a sample of simulated semileptonic $t\bar{t}$ events. Events must contain exactly one lepton with $p_T > 30$ GeV and $|\eta| < 2.1$. Leptons are "dressed" with the surrounding photons within a cone of $\Delta R = 0.1$ and are required to yield an invariant mass within 5 GeV of 80.4 GeV, when combined with a neutrino in the event. The events must also contain at least four jets, reconstructed with the anti-k_T algorithm, with $p_T > 30$ GeV within $|\eta| < 2.4$. At least two of the jets are required to originate from the fragmentation of bottom quarks, and at least two other jets, referred to as light-quark jets, must not originate from bottom quarks. One jet originating from a bottom quark is combined with the lepton and neutrino to form a leptonically decaying top quark candidate, whereas the other jet originating from a bottom quark is combined with two other jets to form a hadronically decaying top quark candidate. The difference in invariant mass of the two top quark candidates is required to be less than 20 GeV, and the invariant mass of the two light-quark jets to be within 10 GeV of 80.4 GeV. If more than one combination of jets satisfy these criteria when combined with the lepton and neutrino, then only one combination is chosen based on how similar the invariant masses of the two top quark candidates are to each other and on how close the invariant mass of the light-quark jets is to 80.4 GeV. The invariant mass of the hadronically decaying top quark candidates constructed in this way for each of the different tune configurations is shown in Fig. 21. The top quark and W boson mass values are obtained from these hadronically decaying top quark candidates by fitting a Gaussian function within an 8 GeV mass window around the corresponding mass peak. Table 5 also contains the differences from the nominal m_t and m_W values (Δm_t, and Δm_W) and the difference in Δm_t^{hyb}, a quantity that was introduced in Ref. [63] to incorporate both an in situ jet scale factor determined from the reconstructed m_W as well as prior knowledge about the jet energy scale in a hybrid approach to extract m_t. Here, Δm_t^{hyb} is approximated as $\Delta m_t - 0.5\Delta m_W$. From Table 5, we observe that the largest deviation from the predictions of CP5 is CP5-CR2 ERD (0.32 GeV) similar to the largest shift found in Ref. [19] using CUETP8M2T4.

6 Summary and conclusion

New sets of parameters for two of the colour reconnection (CR) models implemented in the PYTHIA 8 event generator, QCD-inspired and gluon-move, are obtained, based on the default CMS PYTHIA 8 tune CP5. Measurements sensitive to underlying-event (UE) contributions performed at hadron-colliders at $\sqrt{s} = 1.96$, 7, and 13 TeV are used to constrain the parameters for the CR and for the multiple-parton interactions simultaneously. Different measurements at

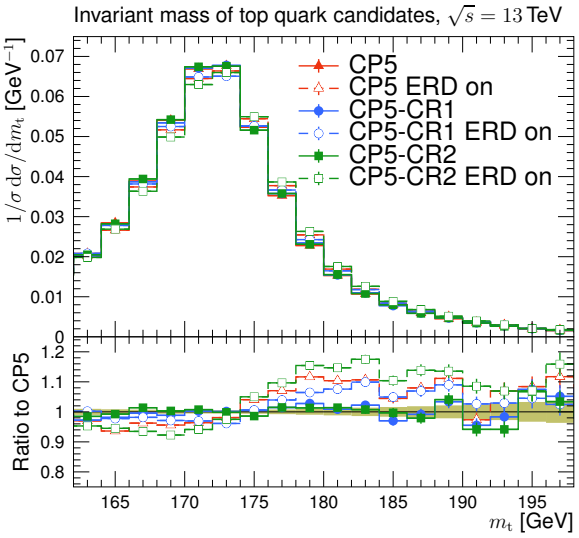

Figure 21: The invariant mass of hadronically decaying top quark candidates for different tune configurations. The coloured band and vertical bars represent the statistical uncertainty in the predictions.

Table 5: The top quark mass (m_t) and W mass (m_W) extracted by a fit to the predictions of the different PYTHIA 8 tunes, along with the differences from the nominal m_t value (Δm_t), m_W value (Δm_W), and Δm_t^{hyb} which represents an estimation of the m_t uncertainty considering the shift in m_W included with a weight of 0.5. The uncertainties in the m_t and m_W values correspond to the uncertainty in the fitted m_t and m_W.

Tune	m_t [GeV]	Δm_t [GeV]	m_W [GeV]	Δm_W [GeV]	Δm_t^{hyb} [GeV]
CP5	171.93 ± 0.02	—	79.76 ± 0.02	—	—
CP5 ERD	172.18 ± 0.03	0.25	80.15 ± 0.02	0.40	0.05
CP5-CR1	171.97 ± 0.02	0.04	79.74 ± 0.02	−0.02	0.05
CP5-CR1 ERD	172.01 ± 0.03	0.08	79.98 ± 0.02	0.23	−0.04
CP5-CR2	171.91 ± 0.02	−0.02	79.85 ± 0.02	0.10	−0.07
CP5-CR2 ERD	172.32 ± 0.03	0.39	79.90 ± 0.02	0.14	0.32

1.96, 7, 8, and 13 TeV, as well as data from e^+e^- colliders are used to evaluate the performance of the new tunes. The central values predicted by the new CR tunes for the UE and minimum-bias events describe the data significantly better than the CR models with their default parameters before tuning. The predictions of the new tunes achieve a reasonable agreement in many UE observables, including the ones measured at forward pseudorapidities. However, the models after tuning do not perform better than the CP5 tune for the observables presented in this study. The new CR tunes are also tested against measurements of strange particle multiplicities for Λ baryons and K^0_S mesons. We show that the new CR models alone do not improve the description of the distribution of the strange particle production as a function of rapidity for Λ baryons. However, we observe that all CP5 tunes, irrespective of the CR model, describe particle production for K^0_S as a function of rapidity well.

The predictions of the new tunes for jet shapes and colour flow measurements done with top quark pair events are also compared with data. All tunes give similar predictions, but none of the tunes describe the jet shape distributions well. Some differences are also observed with respect to the colour flow data, which is particularly sensitive to the early resonance decay option in the CR models. The differences between the predictions using the different tunes

observed here indicate that the inclusion of observables, such as the jet pull angle and other jet substructure observables, could be beneficial in tuning studies. A study of the uncertainty in the top quark mass measurement due to CR effects is also presented, which shows that CR will continue to be one of the dominating uncertainty sources in top quark mass measurements.

References

[1] T. Sjöstrand et al., "An introduction to PYTHIA 8.2", *Comput. Phys. Commun.* **191** (2015) 159, doi:10.1016/j.cpc.2015.01.024, arXiv:1410.3012.

[2] R. Corke and T. Sjöstrand, "Multiparton interactions with an x-dependent proton size", *JHEP* **05** (2011) 009, doi:10.1007/JHEP05(2011)009, arXiv:1101.5953.

[3] A. Buckley et al., "General-purpose event generators for LHC physics", *Phys. Rept.* **504** (2011) 145, doi:10.1016/j.physrep.2011.03.005, arXiv:1101.2599.

[4] G. Gustafson, "Dual description of a confined color field", *Phys. Lett. B* **175** (1986) 453, doi:10.1016/0370-2693(86)90622-2.

[5] Particle Data Group Collaboration, "Review of Particle Physics", *PTEP* **2020** (2020), no. 8, 083C01, doi:10.1093/ptep/ptaa104.

[6] T. Sjöstrand and M. van Zijl, "A multiple interaction model for the event structure in hadron collisions", *Phys. Rev. D* **36** (1987) 2019, doi:10.1103/PhysRevD.36.2019.

[7] T. Sjöstrand, "Colour reconnection and its effects on precise measurements at the LHC", 2013. arXiv:1310.8073.

[8] J. R. Christiansen and P. Z. Skands, "String formation beyond leading colour", *JHEP* **08** (2015) 003, doi:10.1007/JHEP08(2015)003, arXiv:1505.01681.

[9] S. Argyropoulos and T. Sjöstrand, "Effects of color reconnection on $t\bar{t}$ final states at the LHC", *JHEP* **11** (2014) 043, doi:10.1007/JHEP11(2014)043, arXiv:1407.6653.

[10] CMS Collaboration, "Extraction and validation of a new set of CMS PYTHIA8 tunes from underlying-event measurements", *Eur. Phys. J. C* **80** (2020) 4, doi:10.1140/epjc/s10052-019-7499-4, arXiv:1903.12179.

[11] T. Sjöstrand and P. Z. Skands, "Multiple interactions and the structure of beam remnants", *JHEP* **03** (2004) 053, doi:10.1088/1126-6708/2004/03/053, arXiv:hep-ph/0402078.

[12] CMS Collaboration, "Underlying event measurements with leading particles and jets in pp collisions at $\sqrt{s} = 13$ TeV", CMS Physics Analysis Summary CMS-PAS-FSQ-15-007, 2015.

[13] ATLAS Collaboration, "Measurement of charged-particle distributions sensitive to the underlying event in $\sqrt{s} = 13$ TeV proton-proton collisions with the ATLAS detector at the LHC", *JHEP* **03** (2017) 157, doi:10.1007/JHEP03(2017)157, arXiv:1701.05390.

[14] CMS Collaboration, "Measurement of the underlying event activity in pp collisions at the LHC at 7 TeV and comparison with 0.9 TeV", CMS Physics Analysis Summary CMS-PAS-FSQ-12-020, 2012.

[15] ATLAS Collaboration, "Measurement of underlying event characteristics using charged particles in pp collisions at $\sqrt{s} = 900$ GeV and 7 TeV with the ATLAS detector", *Phys. Rev. D* **83** (2011) 112001, doi:10.1103/PhysRevD.83.112001, arXiv:1012.0791.

[16] CDF Collaboration, "Study of the energy dependence of the underlying event in proton-antiproton collisions", *Phys. Rev. D* **92** (2015) 092009, doi:10.1103/PhysRevD.92.092009, arXiv:1508.05340.

[17] CMS Collaboration, "Event generator tunes obtained from underlying event and multiparton scattering measurements", *Eur. Phys. J. C* **76** (2016) 155, doi:10.1140/epjc/s10052-016-3988-x, arXiv:1512.00815.

[18] CMS Collaboration, "Study of the underlying event in top quark pair production in pp collisions at 13 TeV", *Eur. Phys. J. C* **79** (2019) 123, doi:10.1140/epjc/s10052-019-6620-z, arXiv:1807.02810.

[19] CMS Collaboration, "Measurement of the top quark mass with lepton+jets final states using pp collisions at $\sqrt{s} = 13$ TeV", *Eur. Phys. J. C* **78** (2018) 891, doi:10.1140/epjc/s10052-018-6332-9, arXiv:1805.01428.

[20] CMS Collaboration, "Pseudorapidity distribution of charged hadrons in proton-proton collisions at $\sqrt{s} = 13$ TeV", *Phys. Lett. B* **751** (2015) 143, doi:10.1016/j.physletb.2015.10.004, arXiv:1507.05915.

[21] CMS Collaboration, "Measurement of pseudorapidity distributions of charged particles in proton-proton collisions at $\sqrt{s} = 13$ TeV by the CMS experiment", CMS Physics Analysis Summary CMS-PAS-FSQ-15-008, 2016.

[22] A. Buckley et al., "Rivet user manual", *Comput. Phys. Commun.* **184** (2013) 2803, doi:10.1016/j.cpc.2013.05.021, arXiv:1003.0694.

[23] A. Buckley et al., "Systematic event generator tuning for the LHC", *Eur. Phys. J. C* **65** (2010) 331, doi:10.1140/epjc/s10052-009-1196-7, arXiv:0907.2973.

[24] NNPDF Collaboration, "Parton distributions from high-precision collider data", *Eur. Phys. J. C* **77** (2017) 663, doi:10.1140/epjc/s10052-017-5199-5, arXiv:1706.00428.

[25] P. Skands, S. Carrazza, and J. Rojo, "Tuning PYTHIA 8.1: the Monash 2013 tune", *Eur. Phys. J. C* **74** (2014) 3024, doi:10.1140/epjc/s10052-014-3024-y, arXiv:1404.5630.

[26] CMS Collaboration, "Shape, transverse size, and charged hadron multiplicity of jets in pp collisions at 7 TeV", *JHEP* **06** (2012) 160, doi:10.1007/JHEP06(2012)160, arXiv:1204.3170.

[27] ATLAS Collaboration, "Measurement of the jet fragmentation function and transverse profile in proton-proton collisions at a center-of-mass energy of 7 TeV with the ATLAS detector", *Eur. Phys. J. C* **71** (2011) 1795, doi:10.1140/epjc/s10052-011-1795-y, arXiv:1109.5816.

[28] ATLAS Collaboration, "Measurement of the charged-particle multiplicity inside jets from $\sqrt{s} = 8$ TeV pp collisions with the ATLAS detector", *Eur. Phys. J. C* **76** (2016) 322, doi:10.1140/epjc/s10052-016-4126-5, arXiv:1602.00988.

[29] CMS and TOTEM Collaborations, "Measurement of single-diffractive dijet production in proton-proton collisions at $\sqrt{s} = 8$ TeV with the CMS and TOTEM experiments", *Eur. Phys. J. C* **80** (2020) 1164, doi:10.1140/epjc/s10052-020-08562-y, arXiv:2002.12146. [Erratum: doi:10.1140/epjc/s10052-021-08863-w].

[30] CMS Collaboration, "Pseudorapidity distributions of charged particles in pp collisions at $\sqrt{s} = 7$ TeV with at least one central charged particle", CMS Physics Analysis Summary CMS-PAS-QCD-10-024, 2010.

[31] CMS Collaboration, "Measurement of the energy density as a function of pseudorapidity in proton-proton collisions at $\sqrt{s} = 13$ TeV", *Eur. Phys. J. C* **79** (2019) 391, doi:10.1140/epjc/s10052-019-6861-x, arXiv:1812.04095.

[32] CMS Collaboration, "Strange particle production in pp collisions at $\sqrt{s} = 0.9$ and 7 TeV", *JHEP* **05** (2011) 064, doi:10.1007/JHEP05(2011)064, arXiv:1102.4282.

[33] C. Bierlich, G. Gustafson, and L. Lönnblad, "A shoving model for collectivity in hadronic collisions", 2016. arXiv:1612.05132.

[34] C. Bierlich, "Rope hadronization and strange particle production", *Eur. Phys. J. Web Conf.* **171** (2018) 14003, doi:10.1051/epjconf/201817114003, arXiv:1710.04464.

[35] CMS Collaboration, "Measurement of charged pion, kaon, and proton production in proton-proton collisions at $\sqrt{s} = 13$ TeV", *Phys. Rev. D* **96** (2017) 112003, doi:10.1103/PhysRevD.96.112003, arXiv:1706.10194.

[36] CMS Collaboration, "Study of the inclusive production of charged pions, kaons, and protons in pp collisions at $\sqrt{s} = 0.9$, 2.76, and 7 TeV", *Eur. Phys. J. C* **72** (2012) 2164, doi:10.1140/epjc/s10052-012-2164-1, arXiv:1207.4724.

[37] CMS Collaboration, "Study of the production of charged pions, kaons, and protons in pPb collisions at $\sqrt{s_{NN}} = 5.02$ TeV", *Eur. Phys. J. C* **74** (2014) 2847, doi:10.1140/epjc/s10052-014-2847-x, arXiv:1307.3442.

[38] L. Gladilin, "Charm hadron production fractions", 1999. arXiv:hep-ex/9912064.

[39] DELPHI Collaboration, "Tuning and test of fragmentation models based on identified particles and precision event shape data", *Z. Phys. C* **73** (1996) 11, doi:10.1007/s002880050295.

[40] CMS Collaboration, "Measurement of the underlying event activity in inclusive Z boson production in proton-proton collisions at $\sqrt{s} = 13$ TeV", *JHEP* **07** (2018) 032, doi:10.1007/JHEP07(2018)032, arXiv:1711.04299.

[41] J. Alwall et al., "The automated computation of tree-level and next-to-leading order differential cross sections, and their matching to parton shower simulations", *JHEP* **07** (2014) 079, doi:10.1007/JHEP07(2014)079, arXiv:1405.0301.

[42] R. Frederix and S. Frixione, "Merging meets matching in MC@NLO", *JHEP* **12** (2012) 061, doi:10.1007/JHEP12(2012)061, arXiv:1209.6215.

[43] C. Bierlich, G. Gustafson, and L. Lönnblad, "Collectivity without plasma in hadronic collisions", *Phys. Lett. B* **779** (2018) 58, doi:10.1016/j.physletb.2018.01.069, arXiv:1710.09725.

[44] C. Bierlich and J. R. Christiansen, "Effects of color reconnection on hadron flavor observables", *Phys. Rev. D* **92** (2015), no. 9, 094010, doi:10.1103/PhysRevD.92.094010, arXiv:1507.02091.

[45] C. Bierlich, G. Gustafson, L. Lönnblad, and A. Tarasov, "Effects of Overlapping Strings in pp Collisions", *JHEP* **03** (2015) 148, doi:10.1007/JHEP03(2015)148, arXiv:1412.6259.

[46] V. A. Abramovsky, E. V. Gedalin, E. G. Gurvich, and O. V. Kancheli, "Long Range Azimuthal Correlations in Multiple Production Processes at High-energies", *JETP Lett.* **47** (1988) 337.

[47] I. Altsybeev, "Mean transverse momenta correlations in hadron-hadron collisions in MC toy model with repulsing strings", *AIP Conf. Proc.* **1701** (2016) 100002, doi:10.1063/1.4938711, arXiv:1502.03608.

[48] P. Cea, L. Cosmai, F. Cuteri, and A. Papa, "Flux tubes in the SU(3) vacuum: London penetration depth and coherence length", *Phys. Rev. D* **89** (2014) 094505, doi:10.1103/PhysRevD.89.094505, arXiv:1404.1172.

[49] CMS Collaboration, "Measurement of jet substructure observables in $\mathrm{t\bar{t}}$ events from proton-proton collisions at $\sqrt{s} = 13$ TeV", *Phys. Rev. D* **98** (2018) 092014, doi:10.1103/PhysRevD.98.092014, arXiv:1808.07340.

[50] M. Cacciari, G. P. Salam, and G. Soyez, "The anti-k_{T} jet clustering algorithm", *JHEP* **04** (2008) 063, doi:10.1088/1126-6708/2008/04/063, arXiv:0802.1189.

[51] M. Cacciari, G. P. Salam, and G. Soyez, "FastJet user manual", *Eur. Phys. J. C* **72** (2012) 1896, doi:10.1140/epjc/s10052-012-1896-2, arXiv:1111.6097.

[52] M. Dasgupta, A. Fregoso, S. Marzani, and G. P. Salam, "Towards an understanding of jet substructure", *JHEP* **09** (2013) 029, doi:10.1007/JHEP09(2013)029, arXiv:1307.0007.

[53] A. J. Larkoski, S. Marzani, G. Soyez, and J. Thaler, "Soft drop", *JHEP* **05** (2014) 146, doi:10.1007/JHEP05(2014)146, arXiv:1402.2657.

[54] ATLAS Collaboration, "Measurement of colour flow with the jet pull angle in $\mathrm{t\bar{t}}$ events using the ATLAS detector at $\sqrt{s} = 8$ TeV", *Phys. Lett. B* **750** (2015) 475, doi:10.1016/j.physletb.2015.09.051, arXiv:1506.05629.

[55] J. Gallicchio and M. D. Schwartz, "Seeing in color: jet superstructure", *Phys. Rev. Lett.* **105** (2010) 022001, doi:10.1103/PhysRevLett.105.022001, arXiv:1001.5027.

[56] S. Frixione, P. Nason, and G. Ridolfi, "A positive-weight next-to-leading-order Monte Carlo for heavy flavour hadroproduction", *JHEP* **09** (2007) 126, doi:10.1088/1126-6708/2007/09/126, arXiv:0707.3088.

[57] ATLAS, CDF, CMS, and D0 Collaborations, "First combination of Tevatron and LHC measurements of the top-quark mass", Technical Reports ATLAS-CONF-2014-008, CDF-NOTE-11071, CMS-PAS-TOP-13-014, D0-NOTE-6416, FERMILAB-TM-2582-E, 2014. arXiv:1403.4427.

[58] ATLAS Collaboration, "Measurement of the top-quark mass in the fully hadronic decay channel from ATLAS data at $\sqrt{s} = 7$ TeV", *Eur. Phys. J. C* **75** (2015) 158, doi:10.1140/epjc/s10052-015-3373-1, arXiv:1409.0832.

[59] ATLAS Collaboration, "Measurement of the top quark mass in the $t\bar{t} \to$ lepton+jets and $t\bar{t} \to$ dilepton channels using $\sqrt{s} = 7$ tev ATLAS data", *Eur. Phys. J. C* **75** (2015) 330, doi:10.1140/epjc/s10052-015-3544-0, arXiv:1503.05427.

[60] ATLAS Collaboration, "Measurement of the top quark mass in the $t\bar{t} \to$ dilepton channel from $\sqrt{s} = 8$ TeV ATLAS data", *Phys. Lett. B* **761** (2016) 350, doi:10.1016/j.physletb.2016.08.042, arXiv:1606.02179.

[61] ATLAS Collaboration, "Top-quark mass measurement in the all-hadronic $t\bar{t}$ decay channel at $\sqrt{s} = 8$ TeV with the ATLAS detector", *JHEP* **09** (2017) 118, doi:10.1007/JHEP09(2017)118, arXiv:1702.07546.

[62] ATLAS Collaboration, "Measurement of the top quark mass in the $t\bar{t} \to$ lepton+jets channel from $\sqrt{s} = 8$ TeV ATLAS data and combination with previous results", *Eur. Phys. J. C* **79** (2019) 290, doi:10.1140/epjc/s10052-019-6757-9, arXiv:1810.01772.

[63] CMS Collaboration, "Measurement of the top quark mass using proton-proton data at $\sqrt{s} = 7$ and 8 TeV", *Phys. Rev. D* **93** (2016) 072004, doi:10.1103/PhysRevD.93.072004, arXiv:1509.04044.

[64] CMS Collaboration, "Measurement of the top-quark mass in $t\bar{t}$ events with lepton+jets final states in pp collisions at $\sqrt{s} = 7$ TeV", *JHEP* **12** (2012) 105, doi:10.1007/JHEP12(2012)105, arXiv:1209.2319.

[65] CMS Collaboration, "Measurement of the top-quark mass in $t\bar{t}$ events with dilepton final states in pp collisions at $\sqrt{s} = 7$ TeV", *Eur. Phys. J. C* **72** (2012) 2202, doi:10.1140/epjc/s10052-012-2202-z, arXiv:1209.2393.

[66] CMS Collaboration, "Measurement of the top-quark mass in all-jets $t\bar{t}$ events in pp collisions at $\sqrt{s} = 7$ TeV", *Eur. Phys. J. C* **74** (2014) 2758, doi:10.1140/epjc/s10052-014-2758-x, arXiv:1307.4617.

[67] CMS Collaboration, "Measurement of the top quark mass using single top quark events in proton-proton collisions at $\sqrt{s} = 8$ TeV", *Eur. Phys. J. C* **77** (2017) 354, doi:10.1140/epjc/s10052-017-4912-8, arXiv:1703.02530.

[68] CMS Collaboration, "Measurement of the $t\bar{t}$ production cross section, the top quark mass, and the strong coupling constant using dilepton events in pp collisions at $\sqrt{s} = 13$ TeV", *Eur. Phys. J. C* **79** (2019) 368, doi:10.1140/epjc/s10052-019-6863-8, arXiv:1812.10505.

[69] CMS Collaboration, "Measurement of the top quark mass in the all-jets final state at $\sqrt{s} = 13$ TeV and combination with the lepton+jets channel", *Eur. Phys. J. C* **79** (2019) 313, doi:10.1140/epjc/s10052-019-6788-2, arXiv:1812.10534.

[70] CMS Collaboration, "Investigations of the impact of the parton shower tuning in PYTHIA8 in the modelling of $t\bar{t}$ at $\sqrt{s} = 8$ and 13 TeV", CMS Physics Analysis Summary CMS-PAS-TOP-16-021, 2016.

[71] CMS Collaboration, "Measurement of the top quark mass using events with a single reconstructed top quark in pp collisions at $\sqrt{s} = 13$ TeV", *JHEP* **12** (2021) 161, doi:10.1007/JHEP12(2021)161, arXiv:2108.10407.

A Colour reconnection tunes with a leading-order PDF set

The list of input RIVET routines used as inputs for the fits, as well as the centre-of-mass energy values, the η ranges, the names of the distributions, the x-axis ranges, and the R values of the distributions are displayed in Table A.1 for the tunes CP1-CR1 and CP1-CR2, and in Table A.2 for the tunes CP2-CR1 and CP2-CR2. The baseline tunes CP1 and CP2 use the NNPDF31_lo_as_0130 [24] PDF set, with an $\alpha_S(m_Z)$ value of 0.130 for ISR, FSR, and MPI, and the MPI-based CR model. The parameters of the tunes are documented in Ref. [10] and displayed in Tables A.3 and A.4. The parameters obtained from the CP1-CR1, CP1-CR2, CP2-CR1, and CP2-CR2 fits, as well as the value of the goodness of the fits are displayed in Tables A.3 and A.4. The predictions of these new CR tunes for particle multiplicities are shown in Figs. A.1, A.2, and A.3.

Table A.1: List of input RIVET routines, centre-of-mass energy values, η ranges, names of distributions, fit ranges, and relative importance of the distributions used in the fits to derive the tunes CP1-CR1 and CP1-CR2.

				CP1-CR1		CP1-CR2	
RIVET routine	$\sqrt{s}$ [TeV]	$\lvert\eta\rvert$	Distribution	Fit range [GeV]	R	Fit range [GeV]	R
CMS_2015_I1384119	13	<2.0	N_{ch} versus η		1		1
CMS_2015_PAS_FSQ_15_007	13	<2.0	TransMIN charged p_T^{sum}	3–36	1	4–36	0.20
			TransMAX charged p_T^{sum}	3–36	1	4–36	0.20
			TransMIN N_{ch}	3–36	1	4–36	0.20
			TransMAX N_{ch}	3–36	1	4–36	0.20
CMS_2012_PAS_FSQ_12_020	7	<0.8	TransMAX N_{ch}	3–20	1	3–20	0.10
			TransMIN N_{ch}	3–20	1	3–20	0.10
			TransMAX charged p_T^{sum}	3–20	1	3–20	0.10
			TransMIN charged p_T^{sum}	3–20	1	3–20	0.10
CDF_2015_I1388868	2	<0.8	TransMIN N_{ch}	2–15	1	2–15	0.10
			TransMAX N_{ch}	2–15	1	2–15	0.10
			TransMIN charged p_T^{sum}	2–15	1	2–15	0.10
			TransMAX charged p_T^{sum}	2–15	1	2–15	0.10

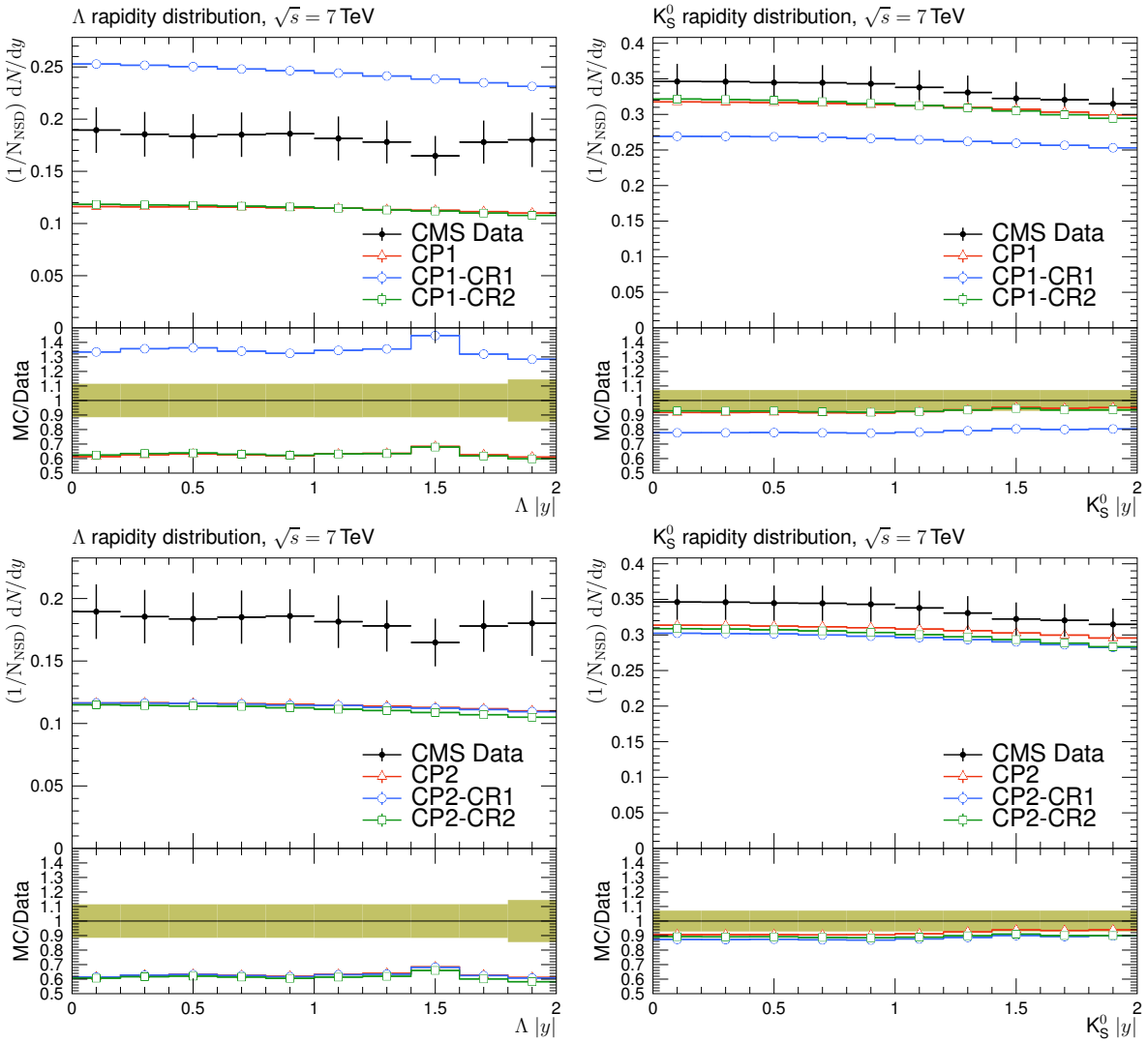

Figure A.1: The strange particle production, Λ baryons (left) and K^0_S mesons (right), as a function of rapidity, measured by the CMS experiment at $\sqrt{s} = 7$ TeV [32]. The predictions of the CP1 and CP1-CR tunes (upper) and CP2 and CP2-CR tunes (lower) are compared with data. The coloured band and error bars on the data points represent the total experimental uncertainty in the data.

Table A.2: List of input RIVET routines, centre-of-mass energy values, η ranges, names of distributions, fit ranges, and relative importance of the distributions used in the fits to derive the tunes CP2-CR1 and CP2-CR2.

				CP2-CR1		CP2-CR2	
RIVET routine	$\sqrt{s}$ [TeV]	$\lvert\eta\rvert$	Distribution	Fit range [GeV]	R	Fit range [GeV]	R
CMS_2015_I1384119	13	<2.0	N_{ch} versus η		0.03		0.05
CMS_2015_PAS_FSQ_15_007	13	<2.0	TransMIN charged p_T^{sum}	5–24	1	5–24	1
			TransMAX charged p_T^{sum}	5–24	0.17	5–24	0.25
			TransMIN N_{ch}	5–24	1	5–24	1
			TransMAX N_{ch}	5–24	0.17	5–24	0.25
CMS_2012_PAS_FSQ_12_020	7	<0.8	TransMAX N_{ch}	5–20	0.07	5–20	0.25
			TransMIN N_{ch}	5–20	1	5–20	1
			TransMAX charged p_T^{sum}	5–20	0.07	5–20	0.25
			TransMIN charged p_T^{sum}	5–20	1	5–20	1
CDF_2015_I1388868	2	<0.8	TransMIN N_{ch}	2–15	0.03	2–15	0.05
			TransMAX N_{ch}	2–15	0.03	2–15	0.05
			TransMIN charged p_T^{sum}	2–15	0.03	2–15	0.05
			TransMAX charged p_T^{sum}	2–15	0.03	2–15	0.05

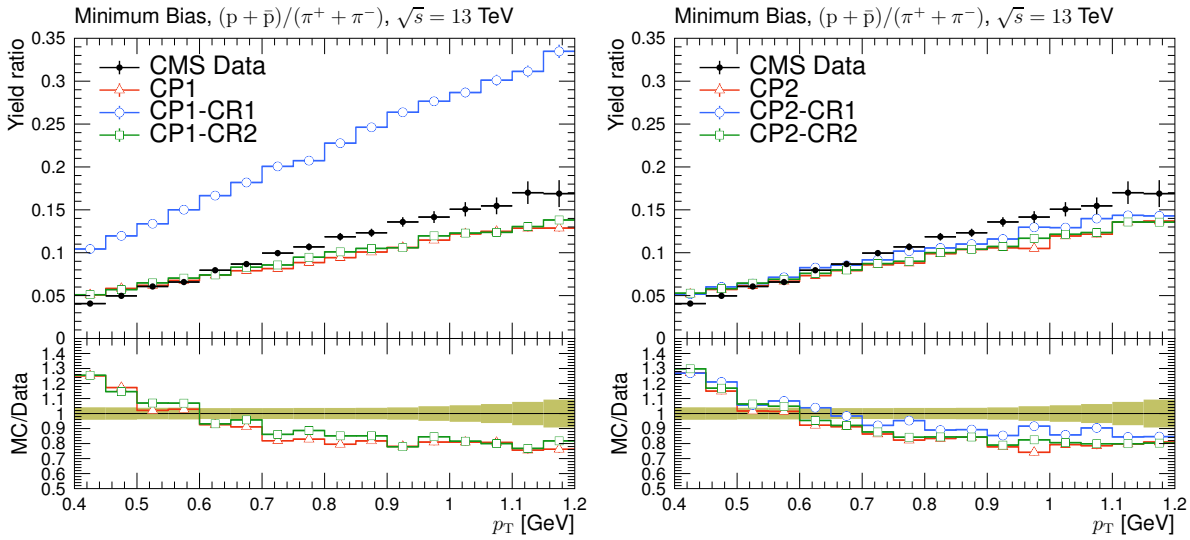

Figure A.2: Ratios of particle yields, p/π, as a function of transverse momentum in MB events, measured by the CMS experiment at $\sqrt{s} = 13$ TeV [35]. The predictions of the CP1 and CP1-CR tunes (left) and CP2 and CP2-CR tunes (right) are compared with data. The coloured band and error bars on the data points represent the total experimental uncertainty in the data.

Table A.3: The parameters obtained in the fits of the CP1-CR1 and CP1-CR2 tunes, compared with the ones of the tune CP1. The upper part of the table displays the fixed input parameters of the tune, while the lower part shows the fitted tune parameters. The number of degrees of freedom (N_{dof}) and the goodness of fit divided by the number of degrees of freedom are also shown.

PYTHIA 8 parameter	CP1 [10]	CP1-CR1	CP1-CR2
PDF set	NNPDF3.1 LO	NNPDF3.1 LO	NNPDF3.1 LO
$\alpha_{\text{S}}(m_{\text{Z}})$	0.130	0.130	0.130
`SpaceShower:rapidityOrder`	off	off	off
`MultipartonInteractions:ecmRef` [GeV]	7000	7000	7000
$\alpha_{\text{S}}^{\text{ISR}}(m_{\text{Z}})$ value/order	0.1365/LO	0.1365/LO	0.1365/LO
$\alpha_{\text{S}}^{\text{FSR}}(m_{\text{Z}})$ value/order	0.1365/LO	0.1365/LO	0.1365/LO
$\alpha_{\text{S}}^{\text{MPI}}(m_{\text{Z}})$ value/order	0.130/LO	0.130/LO	0.130/LO
$\alpha_{\text{S}}^{\text{ME}}(m_{\text{Z}})$ value/order	0.130/LO	0.130/LO	0.130/LO
`StringZ:aLund`	—	0.38	—
`StringZ:bLund`	—	0.64	—
`StringFlav:probQQtoQ`	—	0.078	—
`StringFlav:probStoUD`	—	0.2	—
`SigmaTotal:zeroAXB`	off	off	off
`BeamRemnants:remnantMode`	—	1	—
`MultipartonInteractions:bProfile`	2	2	2
`ColourReconnection:mode`	—	1	2
`MultipartonInteractions:pT0Ref` [GeV]	2.400	1.984	2.385
`MultipartonInteractions:ecmPow`	0.154	0.113	0.165
`MultipartonInteractions:coreRadius`	0.544	0.746	0.587
`MultipartonInteractions:coreFraction`	0.684	0.569	0.533
`ColourReconnection:range`	2.633	—	—
`ColourReconnection:junctionCorrection`	—	8.382	—
`ColourReconnection:timeDilationPar`	—	31.070	—
`ColourReconnection:m0`	—	1.845	—
`ColourReconnection:m2lambda`	—	—	2.769
`ColourReconnection:fracGluon`	—	—	0.979
N_{dof}	183	157	150
χ^{*2}/N_{dof}	0.89	0.73	0.20

Table A.4: The parameters obtained in the fits of the CP2-CR1 and CP2-CR2 tunes, compared with the ones of the tune CP2. The upper part of the table displays the fixed input parameters of the tune, while the lower part shows the fitted tune parameters. The number of degrees of freedom (N_{dof}) and the goodness of fit divided by the number of degrees of freedom are also shown.

PYTHIA 8 parameter	CP2 [10]	CP2-CR1	CP2-CR2
PDF set	NNPDF3.1 LO	NNPDF3.1 LO	NNPDF3.1 LO
$\alpha_{\text{S}}(m_{\text{Z}})$	0.130	0.130	0.130
`SpaceShower:rapidityOrder`	off	off	off
`MultipartonInteractions:ecmRef` [GeV]	7000	7000	7000
$\alpha_{\text{S}}^{\text{ISR}}(m_{\text{Z}})$ value/order	0.130/LO	0.130/LO	0.130/LO
$\alpha_{\text{S}}^{\text{FSR}}(m_{\text{Z}})$ value/order	0.130/LO	0.130/LO	0.130/LO
$\alpha_{\text{S}}^{\text{MPI}}(m_{\text{Z}})$ value/order	0.130/LO	0.130/LO	0.130/LO
$\alpha_{\text{S}}^{\text{ME}}(m_{\text{Z}})$ value/order	0.130/LO	0.130/LO	0.130/LO
`StringZ:aLund`	—	0.38	—
`StringZ:bLund`	—	0.64	—
`StringFlav:probQQtoQ`	—	0.078	—
`StringFlav:probStoUD`	—	0.2	—
`SigmaTotal:zeroAXB`	off	off	off
`BeamRemnants:remnantMode`	—	1	—
`MultipartonInteractions:bProfile`	2	2	2
`ColourReconnection:mode`	—	1	2
`MultipartonInteractions:pT0Ref` [GeV]	2.306	2.154	2.287
`MultipartonInteractions:ecmPow`	0.139	0.119	0.146
`MultipartonInteractions:coreRadius`	0.376	0.538	0.514
`MultipartonInteractions:coreFraction`	0.327	0.599	0.525
`ColourReconnection:range`	2.323	—	—
`ColourReconnection:junctionCorrection`	—	0.761	—
`ColourReconnection:timeDilationPar`	—	13.080	—
`ColourReconnection:m0`	—	1.546	—
`ColourReconnection:m2lambda`	—	—	6.186
`ColourReconnection:fracGluon`	—	—	0.978
N_{dof}	183	117	118
χ^{*2}/N_{dof}	0.54	0.21	0.22

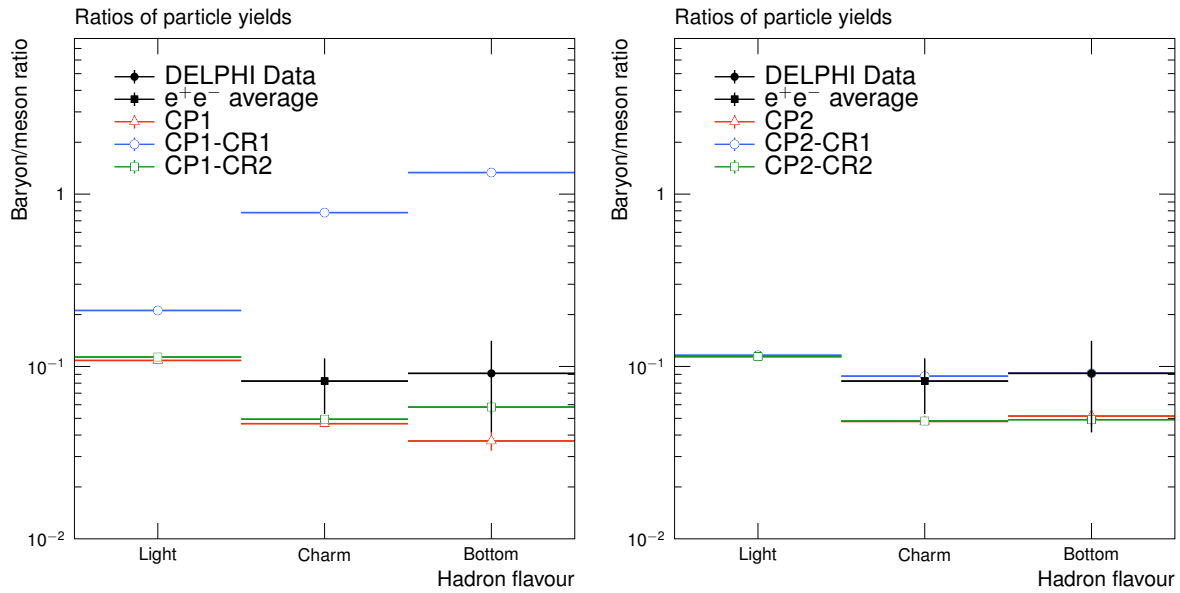

Figure A.3: Ratios of particle yields for light, charm, and bottom hadrons predicted by the different PYTHIA 8 tunes compared with data. The data are compared with predictions from the CP1 and CP1-CR tunes (left) and CP2 and CP2-CR tunes (right). The error bars on the data points represent the total experimental uncertainty in the data.